King Saud University

Arabian Journal of Chemistry

www.ksu.edu.sa
www.sciencedirect.com

ORIGINAL ARTICLE

Effect of number and position of methoxy substituents on fine-tuning the electronic structures and photophysical properties of designed carbazole-based hole-transporting materials for perovskite solar cells: DFT calculations

Nuha Wazzan [a,*], **Zaki Safi** [b]

[a] *King Abdulaziz University, Chemistry Department, Faculty of Science, P.O. Box 42805, Jeddah 21589, Saudi Arabia*
[b] *Al Azhar University-Gaza, Chemistry Department, Faculty of Science, P.O. Box 1277, Gaza, Palestine*

Abstract In perovskite solar cells (PSCs), the state-of-art Spiro-OMeTAD, which used as a hole-transporting material (HTM), suffered from complicated multistep synthesis and difficult purification that make this material cost ineffective, in addition to it being UV-unstable. Thus, new, cost-effective and easy to synthesize small organic molecules is still required. As reported, a carbazole-based compound (R01) was synthesized using a simple two steps method from low-cost commercially available compounds and used as an HTM. R01 exhibited higher conductivity and hole-mobility compared to that of the Spiro-OMeTAD. PSCs fabricated with R01 produced a power conversion efficiency of 12.03%, equivalent to that obtained in devices where Spiro-OMeTAD was the HTM. These findings highlighted R01 as a highly promising HTM with high performance, facile synthesis, and low cost. From a structural perspective, methoxy groups ($-OCH_3$) in the HTM structure are controlling the HOMO level of the compound, apart from the critical role they play in anchoring the material onto the core perovskite layer. In this paper, we report a systematic study of the electronic structures and photophysical properties of twelve designed derivatives of R01. R01 was modified by substituting some hydrogen in the carbazole rings by two, four and six methoxy groups at different positions. The ground and excited state geometries are optimized by applying density functional theory (DFT) and its time-dependent functional (TDDFT), respectively. Detailed investigation of two factors: (i) the number and (ii) position of

---

* Corresponding author.
 E-mail address: nwazzan@kau.edu.sa (N. Wazzan).

Production and hosting by Elsevier

methoxy groups on the frontier molecular orbitals (FMOs), absorption and emission wavelengths, ionization potential, electron affinity, reorganization energies and charge mobility are examined and discussed. The electro-optical and nonlinear optical (NLO) properties are finely tuned in the R01 derivatives. By incorporating methoxy substituents into this carbazole-based compound, systematic design of potential materials for PSCs can be feasible.

1. Introduction

Last few years have witnessed an extensive attraction to use the solar cells to convert the sunlight into electricity at low cost (Stranks et al., 2013; Kazim et al., 2014; Liu et al., 2017). Perovskite solar cells (PSCs) as type of solar cells have been emerged as new systems based on renewable sources. To date, perovskite-type solar cells with and without HTMs have been developed. The cells represent a new class of electrochemical solar cells based on sensitized mesoporous TiO_2 and a liquid electrolyte in a sandwich-like architecture. These cells are known as the most principal rivals for silicon solar cells because of their unique characteristics and high efficiency (Green et al., 2014). Improving the performance of these systems (as light-driven charge separation in molecular systems) to restore as much as possible of the solar energy into electrical current are very intense. These improvements include the design of new and efficient hole-transport materials (HTMs), one of the major constituent of a PSC devise. These materials are solid-state compounds that play important role in extracting holes from perovskites and transport them to the electrode. HTMs are being deposited in the heart of the cell between the perovskite layer and the evaporated metal electrode. The two folds role of the HTMs in the PSC structure are to (1) prevent the direct contact between the perovskite and the metal contact, which minimizes charge recombination and avoids degradation at the metal-perovskite interface and (2) extract positive charges (holes) from perovskite and transport them to the top-electrode (Calió et al., 2016). Additionally, a good hole-mobility (ideally $> 10^{-3} \, cm^2 \, V^{-1} \, s^{-1}$), as well as thermal and photochemical stability are required characteristics of an HTM (Yu and Sun, 2015). Furthermore, transparency in the visible spectrum is desirable to avoid the absorption screen effect toward the active materials/absorber. The physical state of these materials is one of its crucial requirements, in order to prevent the perovskite from dissolution in liquid electrolyte. Solid-state HTMs can be categorized into (1) polymeric (2) inorganic and (3) small organic molecule HTMs. The inorganic HTMs, regardless of their good properties, *i.e.*, high hole mobility and cost effective, suffer from the disadvantage that the solvent used for their deposition can partially dissolve the perovskite, reducing the stability of the device. Polymeric materials have the disadvantages of complex purification process, low solubility, complicated characterization because of their approximate molecular weight, and a poor infiltration into the nanostructured material, this led to many endeavors to design small organic molecules as HTMs (Calió et al., 2016). The classical small organic HTM is Spiro-OMeTAD (Shi et al., 2016). However, Spiro-OMeTAD has some deficiencies like its high-cost, multi-steps synthesis and many purification steps. It is essential to find alternatives of

Spiro-OMeTAD and work in this direction is growing too fast. In this endeavors, experimentalist and theoretical chemists use their techniques to build and test new efficient HTMs (Cai et al., 2017; Zhang et al., 2017a, 2017b; Ansari et al., 2018; Wazzan et al., 2018). The advantage of the theoretical methods over the experimental methods is its convenient and low-cost tool for molecular design, selection and testing of HTMs with higher efficiency. Wang Wo et al. recently introduced a novel high-performance HTM, R01, with a very simple molecular structure, which was synthesized via a facile route with low cost and high yield. R01 is carbazole-based and bridged by 3,4-ethylenedioxythiophene. Its structure is much simpler than not only Spiro-OMeTAD but also other organic HTMs. The much smaller size of the R01 allows a deeper penetration into the mesoporous TiO_2, which facilitates the hole-extraction, thus improving device performance. The perovskite solar cell device using R01 as HTM shows an efficiency (η) of 12.03% and a V_{oc} of 0.98 V under the irradiation of simulated AM1.5G solar light (Wang et al., 2015). In addition, carbazole-based derivatives have attracted much attention as charge-transporting materials for organic light-emitting diodes (OLEDs), dye-synthesized solar cells (DSSCs) and PSCs (Grigalevicius et al., 2006; Salunke et al., 2016). Their interesting photophysical properties such as intense luminescence and reversible oxidation processes, together with the reasonable synthetic costs, the versatility of the carbazole reactive sites and the excellent charge transport properties justify the efforts to find novel solutions for low-cost HTMs for PSCs in this class of compounds (Kang et al., 2015; Yang et al., 2015; Wang et al., 2016a, 2016b; Zhu et al., 2017).

On the other hand, and from a structural point of view, methoxy groups ($-OCH_3$) in the HTM structure are responsible for adjusting the HOMO level of the material, apart from the important role they play in anchoring the material onto the underlying perovskite layer and improve stability and solubility, thus by doing so result in an efficient hole injection (Calió et al., 2016). Since R01 is a very promising alternative HTM in perovskite solar cells, and its facile synthesis may facilitate driving down the fabrication cost of perovskite-based photovoltaic technology, a number of R01 derivatives will be constructed theoretically using the computer software by introducing methoxy groups at different sites in the carbazole donor. Therefore, it is worth developing low-cost HTMs or developing and improving the performance of HTM-free solar cells. The HTM-free solar cell has a much more straightforward structure that is beneficial for reducing the cost. With efforts on the photoanode and back contact interfacial modification, a PCE in the range of 5–8% has been achieved (Jeon et al., 2013a, 2013b; Laban and Etgar, 2013). To provide a simple method to improve the efficiency and stability of planar perovskite solar cells, A copper salts doped 2,2,7,7-tetrakis(N,N-di-p-methoxyphenylamine)-9,9-spi

robifluorene (spiro-OMeTAD) based on a solution processing as the HTM in PSCs was developed (Meng et al., 2016). The incorporation of CuI/CuSCN comprehends a *p*-type doping with efficient charge transfer complex that results in improved film conductivity and hole mobility. Consequently, the PCE is improved from 14.82% to 18.02%. A simple route to control perovskite crystallization and to optimize the interfaces in PHJ PSCs simultaneously and obtaining a maximum power conversion efficiency of 17.06% with improved cell stability was achieved by using branch-shaped perylene film as a seed-mediated under layer, crystalline perovskites with fabric morphology (Wang et al., 2016a, 2016b). Perylene played an important role in the energy-level tailoring of poly(3,4-ethylene dioxythiophene): poly(styrenesulphonate) (PEDOT:PSS) and CH3NH3PbIxCl3–x. In addition, perylene and perovskites form a fully crystalline heterojunction, which is beneficial for minimizing the defect and trap densities. In a similar effort, a seed-mediated method by GeO_2 nano-particles (NPs) for growing crystal perovskite films was developed (Lou et al., 2016). Higher quality of perovskite films was achieved by tuning the size of the GeO_2 NPs, which results in a power conversion efficiency as high as 16.77%. The fabrication and device parameters of inverted planar heterojunction (PHJ) organic–inorganic lead mixed-halide $(CH_3NH_3PbI_3-xCl_x)$ PSCs using a:$CuAlO_2$ as the hole selective buffer layer between the ITO electrode and PEDOT:PSS were demonstrated (Igbari et al., 2016). A short circuit current density (J_{sc}) of 21.98 mA cm^{-2}, an open circuit voltage (V_{oc}) of 0.88 V, a fill factor (*FF*) of 0.75 and a power conversion efficiency (PCE) of 14.52% were achieved for the optimized device.

Therefore, it is necessary to understand the electronic structures of the existing efficient HTMs, in order to be able to build theoretical novel models of R01 derivatives (Jeon et al., 2013a, 2013b). Hence, this study is undertaken to report two issues: The first one is to study in detail the results of theoretical examination of novel R01 compound new design molecules (see Scheme 1). Of particular interest are the structural, molecular orbitals, absorption and emission properties, and hole transport behavior of the newly designed compounds under probe of the parent (R01). The second issue is to study the nonlinear optical properties (NLO) of the compounds under probe to give insight into the photoelectric conversion performance. These properties will be first predicted and characterized by DFT and TDDFT calculations and will be compared with the available experimental data.
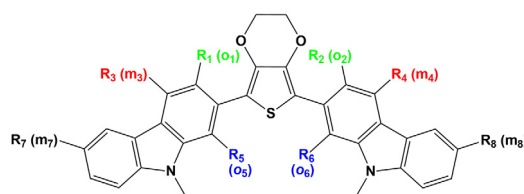
Parent compound: R01: $R_1=R_2=R_3=R_4=R_5=R_6=R_7=R_8=$ H;
5,7-bis(9-ethyl-9H-carbazol-2-yl)-2,3,5,7-tetrahydrothieno[3,4-b][1,4]dioxine

Designed derivatives (Classified according to the number of methoxy groups)

Di-methoxy:

D1: $R_5=R_6=OCH_3$, $R_1=R_2=R_3=R_4=R_7=R_8=$ H
5,7-bis(9-ethyl-1-methoxy-9H-carbazol-2-yl)-2,3,5,7-tetrahydrothieno[3,4-b][1,4]dioxine

D2: $R_1=R_2=OCH_3$, $R_3=R_4=R_5=R_6=R_7=R_8=$ H
5,7-bis(9-ethyl-3-methoxy-9H-carbazol-2-yl)-2,3,5,7-tetrahydrothieno[3,4-b][1,4]dioxine

D3: $R_3=R_4=OCH_3$, $R_1=R_2=R_5=R_6=$H,
5,7-bis(9-ethyl-4-methoxy-9H-carbazol-2-yl)-2,3,5,7-tetrahydrothieno[3,4-b][1,4]dioxine

D4: $R_1=R_4=OCH_3$, $R_2=R_3=R_5=R_6=R_7=R_8=$ H
9-ethyl-2-(7-(9-ethyl-4-methoxy-9H-carbazol-2-yl)-2,3,5,7-tetrahydrothieno[3,4-b][1,4]dioxin-5-yl)-3-methoxy-9H-carbazole

D5: $R_7=R_8=$ OCH$_3$, $R_1=R_2=R_3=R_4=R_5=R_6=$ H
5,7-bis(9-ethyl-6-methoxy-9H-carbazol-2-yl)-2,3-dihydrothieno[3,4-b][1,4]dioxine

D6: $R_1=R_7=$ OCH$_3$, $R_2=R_3=R_4=R_5=R_6=R_8=$ H
9-ethyl-2-(7-(9-ethyl-9H-carbazol-2-yl)-2,3-dihydrothieno[3,4-b][1,4]dioxin-5-yl)-3,6-dimethoxy-9H-carbazole

D7: $R_1=R_8=$ OCH$_3$, $R_2=R_3=R_4=R_5=R_6=R_7=$ H
9-ethyl-2-(7-(9-ethyl-6-methoxy-9H-carbazol-2-yl)-2,3-dihydrothieno[3,4-b][1,4]dioxin-5-yl)-3-methoxy-9H-carbazole

Tetra-methoxy:

T8: $R_1=R_2=R_3=R_4=$ OCH$_3$, $R_5=R_6=R_7=R_8=$ H
5,7-bis(9-ethyl-3,4-dimethoxy-9H-carbazol-2-yl)-2,3-dihydrothieno[3,4-b][1,4]dioxine

T9: $R_1=R_2=R_5=R_6=$ OCH$_3$, $R_3=R_4=R_7=R_8=$ H
5,7-bis(9-ethyl-1,3-dimethoxy-9H-carbazol-2-yl)-2,3-dihydrothieno[3,4-b][1,4]dioxine

T10: $R_3=R_4=R_5=R_6=$ OCH$_3$, $R_1=R_2=R_7=R_8=$ H
5,7-bis(9-ethyl-1,4-dimethoxy-9H-carbazol-2-yl)-2,3-dihydrothieno[3,4-b][1,4]dioxine

T11: $R_1=R_2=R_7=R_8=$ OCH$_3$, $R_3=R_4=R_5=R_6=$ H
5,7-bis(9-ethyl-3,6-dimethoxy-9H-carbazol-2-yl)-2,3-dihydrothieno[3,4-b][1,4]dioxine

Hexa-methoxy:

H12: $R_1=R_2=R_3=R_4=R_5=R_6=$ OCH$_3$, $R_7=R_8=$ H
5,7-bis(9-ethyl-1,3,4-trimethoxy-9H-carbazol-2-yl)-2,3,5,7-tetrahydrothieno[3,4-b][1,4]dioxine

Designed derivatives (Classified according to the position of methoxy groups)

ortho's	D1, D2, T9
ortho-meta	D4, D6, D7, T8, T10, T11, H12
meta's	D3, D5

Scheme 1 Chemical structures and IUPAC names of R01 and its designed derivatives designated as D1-to-D7, T8-T11, and H12 investigated by DFT and TDDFT calculations.

2. Calculations details

DFT and TD-DFT methods were used to investigate the structural, electronic and optical properties of the studied compounds. The more computationally efficient B3LYP density functional Becke-three–Lee–Yang–Parr (B3LYP) (Becke, 1988; Lee et al., 1988) was selected for optimization of the ground state (S_0) and excited state (S_1) geometries of all compounds. The functional has been proved as a suitable method for predicting such geometries/properties (Chen et al., 2014a, 2014b; Bagheri Novir and Hashemianzadeh, 2015; Chi and Li, 2015a, 2015b). The standard 6-31G(d) basis set was used for the optimizations. The use of a 6-31G(d) split-valence double zeta basis set without diffuse functions prevents convergence difficulties in delocalized systems, yet leads to accurate geometries at a reasonable computational cost (Pogantsch et al., 2002; Gao, 2010). The parent hole transporting material (R01) and its twelve designed derivatives (D1 to H12) geometries were optimized with C_1 point group. The optimized geometries show no imaginary frequencies, which ensure energetic minima. The absorption and emission spectra were determined on the optimized S_0 and S_1 geometries, respectively, using TD-B3LYP/6-311 + +G(d,p) level. The total electronic energies of neutral, cationic, and anionic forms of these compounds were used to compute the reorganization energy (λ), the adiabatic (IP_a) and vertical ionization potential(IP_v), the adiabatic (EA_a) and vertical electron affinity (EA_v), the hole extraction potential(HEP) and the electron extraction potential(EEP) at the same level of DFT method, The detailed equations used to calculate these parameters and other parameters could be found in the DFT details in the SD. Computations were performed using the Gaussian 09 program package (Frisch et al., 2016). The composition of molecular orbitals was calculated using the AOMix program (Gorelsky and Lever, 2001; Gorelsky, 2015). Visual inspections were performed using GaussView program (version 5.0.8) (Roy Dennington et al., 2009) and Chemcraft program version 1.8 (build 489) (Zhurko and Zhurko, 2009).

3. Results and discussion

The principal aim of this study is to design and develop new HTMs which have similar chemical structures but different properties to reveal the underlying principles for the future HTMs design.

3.1. Structural features of designed dyes (D1-D7, T8-T11, and H12)

From the parent molecule 5,7-bis(9-ethyl-9H-carbazol-2-yl)-2,3,5,7-tetrahydrothieno[3,4-b][1,4]dioxine (abbreviated as R01), twelve newly derivatives was designed. The derivatives (abbreviated as D1-to-D7) were designed by introducing methoxy groups at the carbazole rings. In D1-D7 (di-methoxy derivatives), two methoxy groups were introduced at different positions at the carbazole rings. In T8-T11 (tetra-methoxy derivatives), four methoxy groups were present. The maximum number of six methoxy groups was introduced in H12 (hexa-methoxy derivative). The common feature in the designed molecules is the presence of electron-rich methoxy substituents

that will improve the contact with the perovskite layer, and by doing so result in an efficient hole-injection (Calió et al., 2016). The chemical structures of the R01 and its designed derivatives along with their IUPAC names are depicted in Scheme 1. On the other hand, the designed molecules could be differentiated according to the positions of the methoxy groups either they are substituted at the *ortho* or at the *ortho* and *meta* position all with respect to the dioxythiophene ring, see Scheme 1. The designed HTMs have a unique general configuration of AD_1-D_1-D_2-D_1-AD_1, which has the carbazole moieties as the significant electron donors (D_1), methoxy groups as an additional electron donor (AD_1), dioxythiophene core as a minor electron donor (D_2), and a repeated unit of D_1, and AD_1.

3.2. Optimized geometries

Parent (R01): The inter-ring distances and the torsional angles in the optimized geometries of the parent molecule (R01) in its neutral, cationic, and anionic states at the ground state (S_o) are collected in Table 1. Fig. 1 represents the HOMOs and LUMOs distribution along with the % contribution to the HOMO and LUMO from different fragments of the HTMs under investigation. Two (R01)/Three (derivatives) main fragments are defined for each molecule. The nature of each fragment as electron-donating/accepting can be demonstrated from its contribution to these orbitals. If the fragment is contributing more to the HOMO than to the LUMO, it is an electron-donating fragment and *vice versa*. As can be seen from Fig. 1, for R01, the two defined fragments are the dioxythiophene core and two carbazole arms. The two fragments are contributing to the HOMO and LUMO; however, dioxythiophene core is contributing with more significant extent to the HOMO than to the LUMO. Dioxythiophene core is contributing by 42% and 36% to HOMO and LUMO, respectively. In contrast, the carbazole arms are contributing with more significant extent to the LUMO (64%) than to the HOMO (58%). Thus, we could conclude that both groups could be considered as an electron-donating group, however, according to the extent of their contributions to the HOMO and LUMO the carbazole arms are the major ones, and dioxythiophene core is the minor one. In the meantime, no X-ray crystal data is available for this compound, we will focus on the effect of the substituted methoxy groups on these geometrical parameters for the same molecule in its different forms, and we will compare between these geometrical parameters in different derivatives, Table 1. The optimized R01 molecule exhibits a non-planar structure with the C1 symmetry, the non-planarity geometries of R01 regulates the packing of the molecule in the solid state and influences the optoelectrical properties of the carbazole-based materials (Iwan and Sek, 2011).

The S–C5 distances are 1.7582, 1.7622, and 1.7817 Å in the neutral, cationic and anionic forms, respectively. These bond distances are elongated in the cationic and anionic forms by 0.004 and 0.024 Å, respectively, compared to that in the neutral form. On the other hand, the C5–C31 distances are shortened in the cationic and anionic forms by 0.027 and 0.032 Å, respectively, compared to that in the neutral form. In the cationic form the electron is removed from the HOMO, and in the anionic form the electron will be added to the LUMO, thus, by visualizing the HOMO and LUMO distribution among the molecule, we can explain the change in the inter-ring distances

Table 1 Bond distances (in Å), bond angles, and torsional angles (in °) of the ground state of R01 and its di-methoxy derivatives (D1-D7) in their neutral, cationic and anionic forms, data in parenthesis belong to the first excited state.

R01		S–C5	C5–C31	S–C5–C31–C32		
neutral		1.7582	1.4637	22.800		
		(1.7752)	(1.4215)	(2.462)		
cationic		1.7622	1.4364	9.168		
anionic		1.7817	1.4316	2.687		

D1		S–C5	C5–C30	S–C5–C30–C31	C31–O66	C32–O66–C68
neutral		1.7592	1.4702	32.699	1.3866	113.856
		(1.7834)	(1.4272)	(17.373)	(1.3800)	(114.133)
cationic		1.7596	1.4456	35.082	1.3491	119.237
anionic		1.7847	1.4389	20.240	1.3950	112.932

D2		S–C5	C5–C30	S–C5–C30–C31	C32–O66	C31–O66–C68
neutral		1.7558	1.4694	47.593	1.3669	118.340
		(1.7790)	(1.4283)	(29.372)	(1.3569)	(119.185)
cationic		1.7596	1.4456	35.082	1.3491	119.237
anionic		1.7804	1.4420	30.897	1.3740	118.435

D3		S–C5	C5–C30	S–C5–C30–C31	C35–O67	C35–O67–C72
neutral		1.7574	1.4645	23.021	1.3659	118.223
		(1.7757)	(1.4214)	(2.357)	(1.3633)	(118.490)
cationic		1.7601	1.4398	11.275	1.3526	118.788
anionic		1.7831	1.4302	2.641	1.3794	117.610

D4		S–C5	C5–C30	S–C5–C30–C31	C35–O71	C35–O71–C72
neutral		1.7579	1.4652	21.994	1.3663	118.199
		(1.7781)	(1.4213)	(1.970)	(1.3614)	(118.530)
cationic		1.7656	1.4385	8.384	1.3518	118.807
anionic		1.7782	1.4338	2.805	1.3792	117.620

D5		S–C5	C5–C27	S–C5–C27–C28	C28–O65	C28–O69–C66
neutral		1.7581	1.4638	23.043	1.3734	118.309
		(1.7966)	(1.4120)	(1.444)	(1.3733)	(118.315)
cationic		1.7615	1.4392	9.989	1.3590	119.263
anionic		1.7811	1.4319	2.900	1.3854	117.765

D6		S–C6	C6–C12	S–C6–C12–C13	C14–O60	C14–O60–C61
neutral		1.7566	1.4692	47.038	1.3815	114.040
		(1.7978)	(1.4259)	(25.717)	(1.3780)	(114.539)
cationic		1.7587	1.4435	35.629	1.3461	119.441
anionic		1.7853	1.4390	27.625	1.3876	114.280

D7		S–C5	C5–C27	S–C5–C27–C28	C29–O60	C29–O60–C61
neutral		1.7568	1.4691	47.074	1.3811	114.089
		(1.7970)	(1.4268)	(26.583)	(1.3777)	(114.573)
cationic		1.7577	1.4431	36.334	1.3495	119.184
anionic		1.7847	1.4395	28.557	1.3872	114.335

(Lin et al., 2003), Fig. 1. A large part of the HOMO (−4.793 eV) is delocalized on the dioxythiophene ring, upon removing of an electron from the HOMO in the cationic form leads to elongation of the S–C5 bond distance. Part of the LUMO (−1.346 eV) is distributed over the C5–C31 (and C5–C11), thus adding an electron to the LUMO results in shortening of these bonds. The shortening of the inter-ring distance in the anionic state is due to the bonding interactions between the π-orbitals on the two carbazole rings. The torsional angle S–C5–C31–C32 that simply resemble the extent of the planarity of the molecule shows a significant decrease by 13.6 and 20.1° in the cationic and anionic forms, respectively, compared to that in the neutral form. Thus, the cationic and anionic forms showed more planner geometries compared to the neutral form, and the anionic form is even more planner than the cationic form. In fact, R01 and its derivatives (as will be

discussed later) exhibit larger geometric deformation between the neutral and ionic forms, this implies that this type of molecules should be p-channel but not n-channel materials (Zhao et al., 2013).

Di-methoxy derivatives (D1-D7): A general notice is that the investigated geometrical parameters (bond lengths and angles) show somehow significant differences between the parent molecule (R01) and its derivatives. It is then evident that the presence of the methoxy groups makes a significant influence on the geometrical structure and subsequently on the electronic properties. On one hand, due to the steric hindrance effect of the methoxy group/s especially for that/those present in the *ortho*-position/s, and on the other hand, due to the electron-accepting (by resonance)/donating (inductively) nature of this group. Comparing the torsional angle S–C5–C31–C32 between the parent molecule (R01) and its derivatives
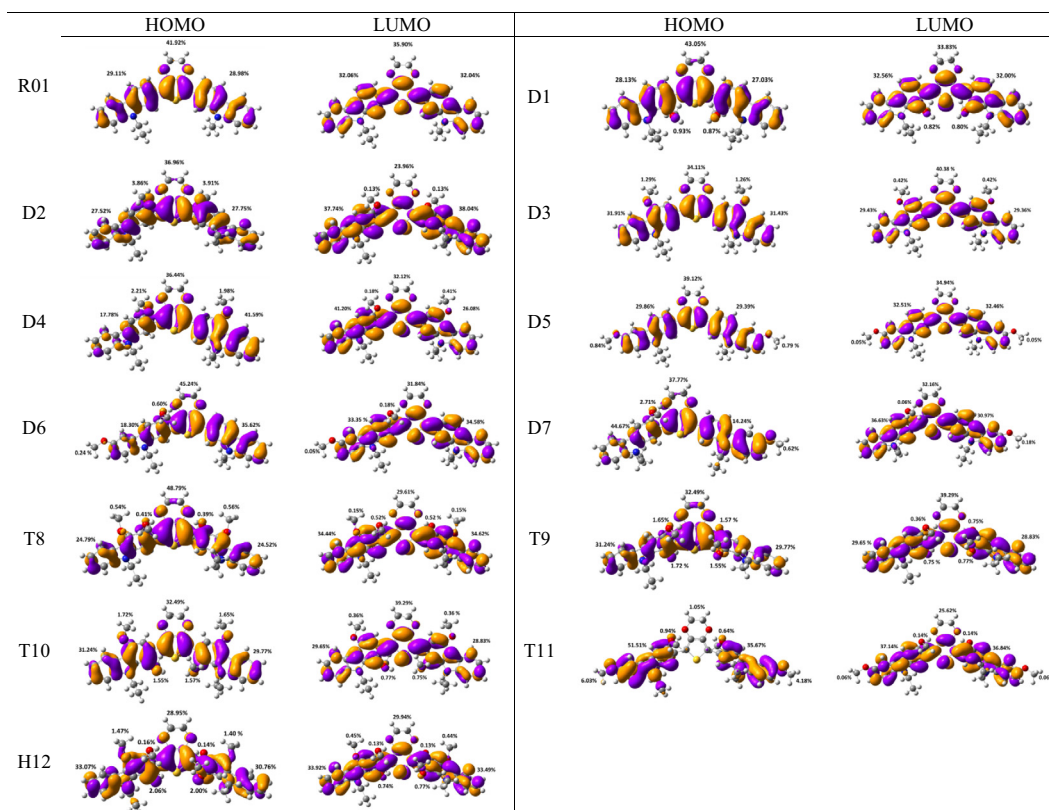
Fig. 1 Electron density isocontours (0.020 au) of HOMO and LUMO orbitals distribution for the ground states of R01 and its methoxy derivatives.

those substituted by two methoxy groups (D1-D7), indicated that the planarity of the R01 is distorted with different extent in its derivatives. For instance, for the derivatives D1, D2, D6, and D7, this dihedral angle is in the range ~33° (D1) to ~47° (D2, D6, and D7) compared to 22.8° for that of R01. On the other hand, the distortion from planarity for the derivatives D3, D4 and D5 is insignificant, since the dihedral angles for these three molecules are very similar to that of R01, ranges from 22.0° (in D4) to 23.0° (in D3 and D5). Thus, the positions of the methyl groups significantly affect the planarity of geometries of the designed derivatives; the positioning of the methoxy group/s at the *ortho*-position/s with respect to the dioxythiophene ring will have a more important steric effect than positioning it/them at the *meta*-position/s (Jeon et al., 2014). For instance, in D3, the two methoxy groups are positioning at the *meta*-positions corresponding to each other at the two carbazole rings, this molecule shows one of the least deviations from planarity and thus a very similar geometry to that of R01. Another notice is that the significant deviation from planarity shown by D1, D2, D6 and D7 derivatives. The displacement of one/two methoxy groups at the *ortho*-position (D1 and D2) and the other one at the phenyl ring of the carbazole ring farthest from the dioxythiophene ring (terminal methoxys), either on the same side (D6) or at the opposite side (D7), seems to enhance the steric effect of the methoxy groups.

The change in inter-ring distances, *i.e.,* S–C5 and C5–C32/C30/C28, shows similar trend showed by the parent molecule (R01). The S–C5 distances are elongated in the cationic and anionic forms compared to that of the neutral form, and the

other bond distances are shortened. The concept used to explain these changes in the R01 can be applied to the designed derivatives. Since the distribution of the HOMO and LUMO on the thiophene ring and on the C5–C12/17/27/30/31 bond does not show significant differences between that of the R01 and those of its derivatives. Additionally, the geometrical parameters of one of the substituted methoxy groups in the derivatives have been tabulated in Table 1. For instance, for the D2 derivative, the C32–O66 bond distance shortened by 0.018 Å in the cationic form and elongated by 0.007 Å in the anionic forms, the C31–O66–C68 bond angle increases by 0.897 in the cationic form and decreases by 0.095° in the anionic forms. From Fig. 1, it is clear that the HOMOs are delocalized with large extent on the substituted methoxy group over the electronegative oxygen atoms, while the LUMOs are distributed with no/less extent. The total % contributions from the methoxy fragments to the HOMO and LUMO orbitals of the investigated HTMs are collected in Table 2. As appeared from Table 2 and Fig. 1, the methoxy groups are contributing more to the HOMOs (range from 0.84 to 7.77%) than to the LUMOs (0.1–1.62%), indicating that the electron-donating nature by resonance is more predominant. The fact that the C–O distances for these derivatives are shortened in cationic form and elongated in anionic form is consistent with the MO pictures (Lin et al., 2003). The distribution of the HOMOs orbitals on the substituted methoxy groups of the derivatives is not the same, while, LUMOs distribution shows similar observation. In other words, the LUMOs are generally not delocalized on these groups indicating their electron-donating nature

Table 2 The % contribution from the methoxy fragments to the HOMO and LUMO.

	D1	D2	D3	D4	D5	D6	D7	T8	T9	T10	T11	H12
HOMO	1.80	7.77	2.55	4.19	1.63	0.84	3.33	1.90	6.49	6.49	11.79	7.23
LUMO	1.62	0.26	0.84	0.59	0.10	0.23	0.24	1.34	2.63	2.24	0.40	2.66

(resonance effect). The HOMOs are delocalized on the oxygen atoms of the methoxy groups, but not on all the substituted methoxy groups. The delocalization of the HOMOs on some methoxy groups indicates that the electron-donating nature of the methoxy group is a predominant effect, and the non-delocalization of them indicates that the electron-withdrawing nature is the predominant effect. Due to the high electronegativity of the oxygen atom; this group could become electron-withdrawing in an inductive sense *via* the σ bonds. Thus, the electron-donating/withdrawing nature of the substituted methoxy group depends on its specific position and interaction with the conjugation system of the phenyl rings. Thus, from MO picture, the methoxy groups that contributed to the HOMO and not contributed to the LUMO, we expected that the C-O bond length would be decreased and increased in the cationic and anionic form, respectively; the expectation is matching the obtained result.

Tetra-methoxy derivatives (T8-T11): In this kind of designed derivatives, four methoxy groups are substituted either at the two (upper) *ortho-* and two *meta-* positions (like in T8), or at the four *ortho-*positions (like in T9), or at the two *meta-* and the two other (lower) *ortho-*positions (like in T10), or finally, at the two *ortho-*positions and the other two methoxy groups are at the phenyl ring farthest from the dioxythiophene ring (like in T11), see Scheme 1 and Table SD 1. Comparing the planarity of T8-T11 and that of the parent molecule (R01) shows that and similar to the effect of some derivatives substituted with two methoxy groups (D1, D2, D6, and D7), the planarity of all of these derivatives are less than that of R01. The S-C5-C28-C28/29 dihedral angle is ranging from 33° (T10)-to-58° (T9). Since the value of this dihedral angle in R01 is 22.008°. On the other hand, the inter-ring distances included the S–C5, and C5–C27/28/31 bond distances of T8-T11 are slightly shortened and elongated, respectively, compared to those of R01. For instance, the S–C5 bond distances are 1.7582 and 1.7565 Å in R01 and T8, respectively, while their C5–C28/31 bond lengths are 1.4637 and 1.4700 Å, respectively, shortening by 0.002 Å and elongation by 0.006 Å.

Supplementary data associated with this article can be found, in the online version, at https://doi.org/10.1016/j.arabjc.2018.06.014.

The anionic forms of these derivatives show significant changes from the geometries of their counterpart neutral forms, while the cationic forms show slightly different geometries of those of the neutral forms. For instance (for T11), the S-C5 bond lengths are 1.7575, 1.7572, and 1.7829 Å in the neutral, cationic and anionic forms, respectively. Thus, it has been slightly shortened by 0.0004 Å and significantly elongated by 0.025 Å in the cationic and anionic form, respectively. Unlike any other derivative, the HOMO (−4.907 eV) of T11 is not delocalized on the S-C5 bond, and like the other derivatives, part of the LUMO (−1.059 eV) is delocalized on the C5–C27 (Fig. 1) thus removing an electron from the HOMO to form

the cationic state should not affect the S-C5 bond length that results in the slight difference that was observed in this bond length in the neutral and cationic form. In contrast, and since the LUMO is delocalized on the C5–C27, adding an electron to the LUMO to form the anionic form would be expected to weaken and thus lengthening this bond as observed.

Hexa-methoxy derivative (H12): The deviation from planarity in this molecule in comparison with R01 is more pronounced, Table SD 2. Since the S−C5−C28−C29 dihedral angle is 56.2 and 22.8°, for H12 and R01, respectively, a difference of ∼33°. This could be easily attributed to the steric hindrance effect of the six substituted methoxy groups. The inter-ring distances (S–C5) are also elongated by 0.006 and 0.027 Å, while the C5–C28 bond distances are shortened by 0.024 and 0.026 Å in the cationic and anionic forms, respectively. The C–O bond distances of the methoxy group are shortened in the cationic forms and elongated in the anionic forms compared to those of the neutral forms, this combined by reverse trend observed in the C–O–C bond angle. In comparison with the neutral forms, the C–O–C bond angles of the methoxy group increase and decrease in the cationic and anionic forms, respectively. Due to the presence of the six methoxy groups (the maximum number of substitution among all derivatives); the HOMO is showing greater delocalization over more substantial parts of the molecule. Four of the methoxy groups are contributing to the HOMO, except the two methoxy groups at the (upper) *ortho-*positions.

Optimized S1 geometries of R01 and its designed derivatives: The inter-ring distances and torsional angles in the optimized geometries of the parent molecule R01 and its designed derivatives at the first excited state (S1) calculated with TDB3LYP/6-31G(d) are collected in Table 1, Table SD 1, and Table SD 2. It was found that the excited state structures are different from the ground state structures. The investigated bond angles, bond angles, and dihedral angles are significantly changed upon excitation. The most interesting observation is that the planarity of the molecule is improved due to the transfer from the ground state to the first excited state; this is evident from the significant decrease in the S−C−C−C dihedral angles, more obviously for R01, D3, and D4. Thus, the excited state structure is more planar than the ground state structure. For instance, the values of S−C−C−C dihedral angles in the ground state change from 22.800, 23.021, and 21.994° to 2.462, 2.357, and 1.970° in R01, D3, and D4, respectively. The modifications of the dihedral angle strongly affect the optical properties of the compounds such as the emission properties and radiative lifetimes (discussed later) (Chitpakdee et al., 2014; Wazzan et al., 2017).

The distribution patterns of HOMOs and LUMOs for R01 and of its derivatives in the first excited states (S1) have been shown in Fig. 2. Unlike R01 and other derivatives, T11 derivative shows the significant difference in the HOMO distribution (and not the LUMO) between the S0 and S1. In the HOMO of the excited state, the electronic charge is delocalized over a
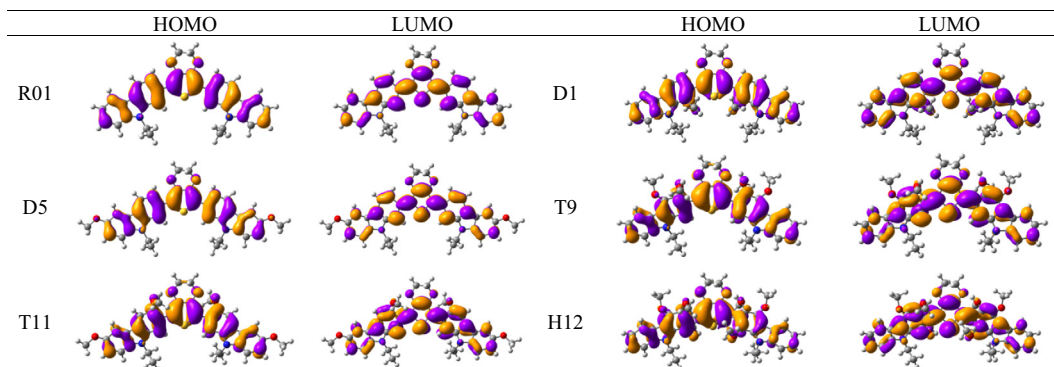
Fig. 2 HOMO and LUMO orbitals distribution for the first excited state (S₁) of some investigated HTMs as representative examples.

region that was not covered by the HOMO in the ground state geometry, *i.e.*, the dioxythiophene core. Thus, at the S₁ the HOMO is distributed over more substantial parts of the molecule. We found general intramolecular charge transfer (ICT) in all investigated HTMs for S₀ as well as the S₁ state.

3.3. Frontier molecular orbital

In the present study, we have carried out a systematic quantum chemical calculations using density functional theory DFT to estimate the electronic and optical properties for 5,7-bis(9-ethyl-9H-carbazol-2-yl)-2,3,5,7-tetrahydrothieno[3,4-b][1,4]dioxin and some of its new designed methoxy derivatives (Scheme 1), which they may be used as an efficient HTMs in the perovskite solar cells. As is known examination of the frontier molecular orbitals (FMOs) is vital to understand the electronic structures of chemical compounds. In addition, FMOs are the backbone factors to illustrate the carrier transport properties of the molecules, which affect the electronic, optical, and conducting properties of materials. By controlling the HOMO and LUMO levels, it is feasible to design materials for PSCs with desirable charge carrier transport properties (Chen et al., 2014a, 2014b). Therefore, examination of HOMOs and LUMOs of the newly designed compounds is

highly useful, by which a reasonable qualitative indication of the ability of charge injection and transport can be estimated by knowing the relative ordering of HOMOs and LUMOs. The calculated distribution patterns of the highest occupied molecular orbitals (HOMOs) and lowest unoccupied molecular orbitals (LUMOs) and the energy levels for the ground states of the parent compound and its new design derivatives are plotted in Fig. 3. For the parent compound (R01), as sketched in Fig. 3, the HOMO and LUMO are almost distributed over the whole molecule, indicating that the molecule possesses π-features. A good delocalization of HOMO is favorable to enhancing the hole transfer integral (Zhang et al., 2017a, 2017b). Similarly, other twelve designed molecules exhibit the same results with some exceptions. These exceptions mainly depend on the position and the number of the substituted methoxy groups. For example, new designed compound D4, the HOMO is located on the central and left-hand side of the molecule, and it has a very weak localization on the right-hand side of the molecule, while the LUMO is almost localized on whole the molecule. For D6 and D7 molecules, the indole group on the right-hand side have a week contribution to the HOMOs, while the LUMOs of these molecules are almost localized overall the backbone of the molecule. These results can be attributed to the position of the methoxy groups. In
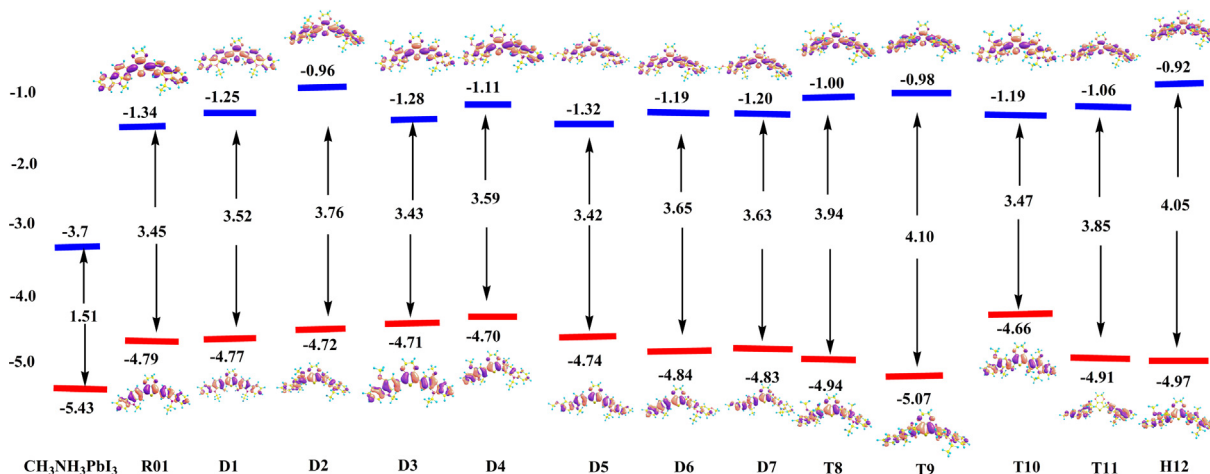
Fig. 3 The calculated molecular orbitals for molecule R01 and its newly designed derivatives P1-D7 (blue ones are LUMOs and red ones are HOMOs), using DFT at the B3LYP/6-31G(d) level. HOMO and LUMO energies are in eV. Energy gap values are given in the middle part of the Fig (eV). Value ranges from (−0.2)-to-0.2 eV.

D6 molecule, two methoxy groups are substituted on the carbazole unit, which located on the left-hand side of the molecule. On the other hand, in D7 molecule, the two methoxy groups are substituted on both carbazole units. As is known the methoxy substituent actually impacts the ring electronics via two competing effects. The oxygen's lone pair is well-placed to delocalize and increase electron density within the ring's conjugated system. This allows delocalization to better stabilize positive charges. So the methoxy is electron-donating from a resonance perspective. Additionally, because oxygen is quite electronegative, the methoxy group is electron-withdrawing in an inductive sense via the σ bonds. As can be seen from the distribution of the HOMOs and LUMOs the resonance donation is much stronger than the inductive sense.

Chi and Li (2015a, 2015b) suggested that the excellent HOMO delocalization is favorable for hole transport and hole transfer integral. As compared with the hole-transport, they have the relative inferior electron transport possibility that is determined by the delocalization of the LUMO. The result of FMO analysis suggests that the parent R01 and most of the designed molecules have good hole-transport properties, and consequently they may be very useful potential candidates as HTMs. Previous studies (Minaev et al., 2012; Baryshnikov et al., 2012) reported that the central principle of HTM in perovskite is similar with that of electron transfer to TiO$_2$ surface in DSSC except that the electron is injected in the latter.

In order to understand the influence of the electronic properties of the R01 compound and the newly designed molecules, the analyzing of the values of HOMO energies (E_{HOMO}), LUMO energies (E_{LUMO}) and the energy gap ($\Delta_{H-L} = E_{LUMO} - E_{HOMO}$) are considered. As is known the HOMO energy level of HTM should be higher than the valence band of perovskite (Zhang et al., 2017a, 2017b), and the lower HOMO level that is much closer to the valence band of the mixed perovskite (−5.65 eV) would results in efficient hole extraction and overall PCE of the devices (Rakstys et al., 2015).

Table 3 and Fig. 3 summarize the DFT B3LYP/6-31(d) values of E_{HOMO}, E_{LUMO}, Δ_{H-L} energies, as well as the available experimental data (Wang et al., 2015). It should be mentioned that solid-state packing effects are not included in the DFT calculations, which tend to affect the HOMO and LUMO energy levels in a thin film compared to an isolated molecule as considered in the calculations (Mandal et al., 2017). However, according to Table 3 the calculate HOMO energy level of R01 (−4.79 eV) is in a good agreement with the experiment value (−5.30 eV) (Wang et al., 2015) revealing the constancy of theoretical results calculated at B3LYP/6-31(d) level. It is important to note that the HOMO of R01 is much more positive than that of the conduction band of mixed-perovskite (−5.44 eV) (Bi et al., 2016) and CH$_3$NH$_3$PbI$_2$ perovskite (−5.44 eV) (Krishnamoorthy et al., 2014; Vivo et al., 2017). Taken the HOMO of the R01 as a reference, as a general, the HOMO energy level is increased (destabilized) when two methoxy groups were substituted (ranges from −4.70 to −4.79 eV), the exception are D6 (−4.84 eV) and D7 (−4.83 eV). On the other hand, the introduction of four and/or six methoxy substituents results in decreasing the HOMO (stabilization) (ranging from −4.94 to (−5.07 eV)), except of T10 (−4.66 eV). These indicate that di-methoxy substitution leads to destabilize (higher) HOMO level and generally the di-methoxy derivatives are losing their electrons more easily, which implies the higher hole injection or transporting ability, while the tetra-/hexa-methoxy derivatives should be more chemically stable (Zhang et al., 2012a, 2012b).

Generally, the open-circuit voltage (V_{oc}) values of all the designed HTMs decreased (except T10), as the number of methoxy groups increased. Since, the V_{oc} values of the di-methoxy derivatives is in the range 0.586–0.724 eV, for tetra-methoxy derivatives the values are in the range 0.335–0.523 eV, and it is only equals to 0.460 eV for H12 (derivative with hexa-methoxy). We could say that as the number of methoxy groups increased as the electron recombination would be enhanced. The elevation of HOMO energy level would result in a high V_{oc} the value that is determined by the difference between the HOMO level of HTMs and quasi-Fermi levels

Table 3 The FMOs energies of E$_{HOMO}$, E$_{LUMO}$, HOMO–LUMO Gaps (Δ_{H-L}) calculated by DFT and the lowest excited energies (E$_g$), first singlet excitation and excitation binding energies (in eV) at the B3LYP/6-31G(d) level. Note: in parenthesis are the experimental data from reference (Wang et al., 2015).

HTM	E_{HOMO}	Gaussian E_{LUMO}	Gaussian Δ_{L-H}	E_g	Calculated E_{LUMO}	Calculated Δ_{L-H}	E_1	Gaussian E_b	Calculated E_b	V_{oc}
R01	−4.793 (−5.30)	−1.346 (−2.42)	3.447 (2.88)	3.000	−1.791	3.002	2.522	0.447	0.002	0.637 (0.86)
D1	−4.771	−1.252	3.519	3.060	−1.709	3.062	2.560	0.459	0.002	0.659
D2	−4.724	−0.962	3.763	3.200	−1.528	3.196	2.606	0.563	−0.004	0.706
D3	−4.706	−1.279	3.427	2.990	−1.711	2.995	2.490	0.437	0.005	0.724
D4	−4.703	−1.111	3.592	3.090	−1.610	3.092	2.535	0.502	0.002	0.727
D5	−4.741	−1.316	3.424	3.067	−1.671	3.069	2.460	0.357	0.002	0.689
D6	−4.844	−1.195	3.649	3.247	−1.598	3.246	2.532	0.402	−0.001	0.586
D7	−4.828	−1.199	3.629	3.220	−1.607	3.221	2.532	0.409	0.000	0.602
T8	−4.939	−0.995	3.944	3.482	−1.456	3.483	2.651	0.462	0.001	0.491
T9	−5.075	−0.979	4.096	3.599	−1.470	3.605	2.732	0.497	0.006	0.355
T10	−4.662	−1.189	3.473	3.091	−1.570	3.092	2.467	0.382	0.001	0.768
T11	−4.907	−1.059	3.848	3.403	−1.500	3.407	2.567	0.445	0.004	0.523
H12	−4.970	−0.923	4.047	3.476	−1.497	3.473	2.697	0.571	−0.003	0.460

of TiO_2 or the valence band of perovskite (-5.65 eV), a bigger difference implies a higher open-circuit voltage, indicating that the HTM has an efficient hole extraction capability (Jeon et al., 2013a, 2013b; Chi et al., 2016; Zhang et al., 2017a, 2017b). Indeed, the HOMO energy level of new designed molecule T10 (-4.66 eV), which is ~ 0.13 eV higher than the parent compound (R01) has the largest V_{oc} (0.768 eV), T10 The lowest HOMO level (-5.075 eV) is reported for T9 (with four substituted methoxy groups), it is found to be the deepest one which mean that T9 based on PSCs would have the lowest V_{oc} (0.355 eV), Table 3, than the other molecules (Liu et al., 2016), however it is still more positive than the mixed and $CH_3NH_3PbI_2$ perovskite. This is followed by the HOMO level of H12, the *hexa*-methoxy derivative. H12 has HOMO energy of -4.970 eV and V_{oc} value of 0.460 eV.

The calculated V_{oc} values collected in Table 3, shows that the decreasing order of V_{oc} when comparing the R01 with the di-methoxy derivatives is D4 (0.727 eV) > D3 (0.724 eV) > D2 (0.706 eV) > D5 (0.689 eV) > P1 (0.659 eV) > R01 (0.637 eV) $\geq$ D7 (0.602 eV) > D6 (0.586 eV), and with the tetra-methoxy derivatives is T10 (0.768 eV) > R01 (0.689 eV) > P9 (0.523 eV) > T8 (0.0491 eV) > T9 (0.0355 eV), and the *hexa*-methoxy derivative (H12) has lower V_{oc} value by 0.229 eV compared to that of the parent. As reported, the open-circuit voltage values are only quantitative, since the applied model does not consider the kinetics of back electron transfer. Most of the designed HTMs have larger V_{oc} values (and higher HOMO energies) compared to the parent molecule, that demonstrated the effect of the number and position of substituted methoxy groups that may retarded the back electron transfer, hence improving the open-circuit voltage (Mandal et al., 2017).

Wang et al. showed that for a proper HTM material, the LUMO energy level should be higher than the conduction band of perovskite to inhibit the electron in perovskite back to metal electrodes (Liu et al., 2016). The lower LUMO effectively blocks the electron transport from the perovskite to the Au contact, and this causes an increase in the fill factor (FF) value and thus an enhanced PCE (Calió et al., 2016). Almost all of the calculated LUMO energy level values are located between the E_{HOMO} of MAPbI$_3$ (5.45 eV) and Au anode (5.10 eV), indicating the efficient hole-transporting processes in the PSCs devices.

According to Table 3 and Fig. 3, the LUMO energy levels of the newly designed molecules are estimated to be destabilized (more positive) than the that of $CH_3NH_3PbI_3$ perovskite (-3.91 eV). In addition, our results show that the energy difference between the LUMO energy level and the conduction band of $CH_3NH_3PbI_3$ perovskite is ranged from 2.14 eV to 2.47 eV (Table 3), which is enough to block the charge recombination. Based on the above results, the new designed HTMs are assumed to not only perform as a hole transporting layer but also play as an electron blocking layer in the PSCs, leading to the reduction of an electron from perovskite layer and hole from hole-transporting layer (Liu, Zhu et al.). In order to explore the cause of the HOMO destabilization (energy raised) of most of the di-methoxy derivatives and the cause of its stabilization (energy lowered) for most of the tetra- and *hexa*-methoxy derivatives, also the cause of LUMO destabilization (energies lowered) in all derivatives, we make an analysis on the molecular orbital population, Fig. 1. Fig. 1 indicates

the total % contributions of the substituted methoxy groups (% $\sum$). The methoxy groups in the di-methoxy derivatives (except D6 and D7) contribute mainly to the HOMO orbitals, their contributions are in the range from 1.6 to 7.8%, in the tetra- and *hexa*-methoxy derivatives (except T10), the methoxy substituents contribute also to the HOMO, but the total contributions are more significant, and it is in the range 1.9–11.8%. The total % contributions to the LUMOs from these groups in all derivatives is less significant and in the range 0.1–2.7%. Clearly, the substituent contributes more to the HOMO than the LUMO in these compounds. Hence, the decrease of HOMO energies in tetra- and hexa-derivatives and the increase of LUMO energies in all derivatives is mainly attributed to the enhanced electron delocalization that arise from the electron lone pair of an oxygen atom (of methoxy) leads to resonance. Thus, the resonance effect will overcome the inductive effect due to high electronegativity of the oxygen atoms, as evident from HOMO and LUMO distribution pattern (Zhao et al., 2013).

To overcome the electron-injection barrier energy in R01, 3.754 eV (E_{LUMO} (R01) –W (gold) = $-1.346 - (-5.1) = 3.754 eV$), would be required; the work function (W) of gold is -5.1 eV, and the E_{LUMO} level of R01 is -1.346 eV, Table 3. On the other hand, to overcome the hole-injection barrier energy in R01, 1.057 eV ($E_{HOMO}(R01) - (-5.85) = -4.793 - (-5.85) = 1.057 eV$) would be required (Irfan et al., 2015). To overcome the electron-injection barrier energy for all new designed derivatives with higher LUMO levels (ranges from -0.923 to -1.316 eV) are smaller than that of R01, indicating that these compounds may not apply to electron-injection materials, but they may be good hole-injection materials as R01 because of their significantly high HOMO levels (Chen et al., 2014a, 2014b). Additionally, to overcome the electron-injection barrier energy for the designed derivatives (D1, D2, D3, D4, D5, D6, D7, and T10), with higher HOMO levels, ranges from -4.828 to -5.075 eV), are larger than that of R01. It is anticipated that the designed derivatives (except T8, T9, T11, and H12 derivatives) would be a superior hole-transport material than the parent compound.

As is known the magnitude of the HOMO-LUMO gap has significant chemical implications, even if qualitatively evaluated. A large gap implies good thermodynamic stability of the compound, whereas a small gap suggests an easy electronic transition. Inspection of Table 3. indicates that the energy gaps, Δ_{H-L}, of a new designed systems are found to be higher than the parent molecule, except of D3 and D5 molecules. The highest electronic energy gap is attributed to the T9 molecule, which contains four substituted methoxy groups, while the lowest one, which results from a more extended conjugation, is corresponded to D3 in which only two methoxy groups are introduced. In general, this means that introduction of methoxy groups increases the thermodynamic stability of the system in comparison to the parent molecule. Indeed, the thermodynamic stability increases as the number of methoxy groups increases. These results may be attributed to the presence of the lone pair of an electron on the oxygen, which release the electron towards the π-bond, through resonance, raising the energy of frontier molecular orbitals. The trend of the energy gap Δ_{H-L} is as: T9 > T8 > H12 > T11 > D6 > D7 > D2 > D4 > T10 > D1 > R01 > D3 > D5. The Δ_{H-L} value of each investigated molecule is larger than its

corresponding E_g value, mainly due to the neglect of interelectronic interaction upon the single one-electron excitation in estimating Δ_{H-L}, however, the variation trend is similar (Chen et al., 2014a, 2014b).

3.4. Absorption and emission energy

It is worth mentioning that there are no experimental data for newly designed compounds because they have never been synthesized except for the parent molecule R01, which has been described in reference Wang et al. (2015). In order to adventure the properties of electronically excited states of the studied compounds, electronic transitions, the calculated absorption and emission spectra, λ_{abs} and λ_{em} (in nm), the excitation energies, the oscillation strengths (f) and their assignments are calculated for each molecule using TD-B3LYP/6-311 + +G(d, p)//B3LYP/6-311 + +G(d,p) level of theory. The calculated results are presented in Table 4, together with the available experimental results. An important feature of HTMs is their light absorbance in the near UV-region, between 300 and 400 nm, thus avoiding competition with perovskite absorption (Calió et al., 2016). It is worth mentioning that in some cases (R01, D1, D2, D3, D4, and H12) the purely electronic transition HOMO → LUMO is observed, the $S_0 \to S_1$ electronic transitions in these compounds are combined by the larger oscillation strengths, indicating that these transitions are strongly allowed. On the other hand, in other cases (D5, D6, D7, and T10), the $S_0 \to S_5$ electronic transitions are the transition with maximum f values; these are due to HOMO/HOMO-1/HOMO-2 to LUMO, indicating the small energy differences between HOMO, HOMO-1, and HOMO-2. In T8 and T9 derivatives, the $S_0 \to S_7$ electronic transitions are predominately by HOMO to LUMO with f values of 1.00 and 0.83, respectively. In the case of T11, $S_0 \to S_8$ is dominated by HOMO-2 → LUMO transition.

It is apparently evident from Table 4 that all electronic transitions are π-π^* type, and no localized electronic transitions are shown among the calculated singlet-singlet transition.

In addition the oscillator strength for S_0-S_1 attributed to HOMOLUMO transition for all compounds leading to maximum absorption was also noted. According to Table 4, the high values of the oscillator strength (f) (0.47–1.29) indicate that the electronic transitions of π-π^* type are strongly allowed. It is obvious from Table 4 that the calculated maximum absorption wavelength, λ_{abs}, of R01 compound (413 nm) moderately agrees with the experimental results (360 nm) (Wang et al., 2015). As compared with R01, the λ_{abs} values of all new designed molecules are blue shifted (and in the range 357–405 nm), except of D3 molecules, which is red shifted by only 1 nm (λ_{abs} = 414 nm). It is also observed that the λ_{abs} of the di-methoxy molecules lies between 382 and 414 nm, meaning that it is limited to the visible region. The compound D3 shows the longest wavelength absorption at 414 nm, which was considerably red shifted in comparison to that of the parent compound (R01) (413 nm). For compounds with two substituted methoxy groups (D1, D2, D4, D5, D4, D2 and D7), our results note a maximum absorption wavelength in the visible region (382–405 nm), which were considerably blue shifted compared to R01. The results imply that for all derivatives the absorption takes place outside or close to the visible region and overlaps slightly with the absorption band of perovskites (Chi et al., 2016). Moreover, we found a blue-shift and a decrease in the absorption intensity in the near UV/UV region in the order T9 (344 nm) → T8 (356 nm) → H12 (357 nm) → T11 (364 nm), as presented in Table 4, which is consistent with the energy gap trend. Thus, the presence of the methoxy groups would decrease the electron donating ability of the carbazole ring/s, maybe to the predominant inductive effect of electronegative oxygen atoms, and shortened π-electron delocalization over the whole molecule, which blue-shifted the absorption maxima, compared with that of R01 (Kim et al., 2015). However, the number, and position of methoxy groups attached to the carbazole ring had a marginal effect on the maximum absorption of the dyes.

The conclusion can be derived from above that T10 with four-methoxy shows longer (λ_{abs} = 401 nm) but stronger

Table 4 The absorption λ_{abs}/emission λ_{em} wavelengths (in nm) based on the S_0 and S_1 states, respectively, along with the radiative lifetime (in ns), Stocks shifts λ_{ss} (in nm), and light harvesting efficiency (**LHE**) at the TD-B3LYP/6-311 + +G(d,p). Note: in parenthesis are the experimental data from reference (Wang et al., 2015).

HTM	Excitation	λ_{abs}	f_{abs}	Assignment	LHE	λ_{em}	f_{em}	Assignment	τ	λ_{ss}
R01	$S_0 \to S_1$	413 (360)	1.29	H → L (70%)	0.949	465 (467)	1.34	H ← L (70%)	2.557	52
D1	$S_0 \to S_1$	405	1.23	H → L (70%)	0.941	454	1.32	H ← L (70%)	2.569	49
D2	$S_0 \to S_1$	388	0.83	H → L (70%)	0.852	476	1.17	H ← L (70%)	2.897	88
D3	$S_0 \to S_1$	414	1.18	H → L (70%)	0.934	498	1.32	H ← L (70%)	2.821	84
D4	$S_0 \to S_1$	401	0.95	H → L (70%)	0.888	453	1.11	H ← L (70%)	2.927	52
D5	$S_0 \to S_5$	404	1.19	H-2 → L (11%)	0.935	504	1.52	H → L (70%)	2.509	100
				H → L (69%)						
D6	$S_0 \to S_5$	382	1.18	H → L (70%)	0.934	490	1.44	H → L (71%)	2.502	108
D7	$S_0 \to S_5$	385	0.83	H-1 → L (11%)	0.852	490	1.40	H → L (70%)	2.567	105
				H → L (69%)						
T8	$S_0 \to S_7$	356	1.00	H → L (70%)	0.900	468	1.27	H ← L (70%)	2.574	112
T9	$S_0 \to S_7$	344	0.83	H → L (70%)	0.852	454	1.13	H ← L (70%)	2.724	110
T10	$S_0 \to S_5$	401	1.04	H → L (70%)	0.909	503	1.33	H ← L (70%)	2.851	102
T11	$S_0 \to S_8$	364	0.68	H-2 → L (55%)	0.791	483	1.34	H ← L (71%)	2.609	119
				H-1 → L (28%)						
				H → L (29%)						
H12	$S_0 \to S_1$	357	0.47	H → L (68%)	0.661	460	1.07	H ← L (70%)	2.971	103

maximum absorption wavelength(f = 1.04 nm), compared to those of other four/six methoxy substituents, although the methoxy groups in T10 and T8 are in the *ortho-ortho- and meta-meta* (in T8 they are at o1o2m3m4 and T10 they are at o5o6m3m4), see Scheme 1, this indicates that the particular position of the methoxy group/s has a major effect on the electronic properties of these compounds. These results lead us to estimate that increasing the number of substituted methoxy groups leads to blue shift, whereas, introduction two methoxy groups keeps the λ_{abs} in the visible region. As a result, the number and position of methoxy groups introduced on the carbazole ring/s affected the electron distributions, which may have contributed to the hypsochromic shift of the absorption spectrum, and the decreasing of the oscillation strengths.

3.5. Light harvesting efficiency

The ability of the materials and the molecules to capture photons of solar light is called as light harvesting efficiency (LHE). Higher the value of f, higher is the light capturing ability. The LHEs of the parent is comparable to those of some of its derivatives, however, it has the largest value (0.949). Among the derivatives, D1, D3, D5, D6, T8, and T10 are the derivatives with comparable LHE values to that of R01, the difference is not more than 0.05. In contrast, the other derivatives especially H12 show significant lower LHE values in comparison to those of the former derivatives and to that of R01. For instance, the difference reaches 0.28 in case of H12.

3.6. Emission properties

In this study TD-DFT//B3LYP/6-31G(d) has been performed for optimized structures on an excited state to simulate the emission spectra of the compounds under study where the first singlet excited states are listed in Table 4. In all cases and similar to the absorption spectra, S_1-S_0 fluorescence peaks in emission spectra have the largest oscillator strengths in all molecules, and ~70% arises predominantly from LUMO → HOMO transition. Based on Table 4, the calculated maximum emission wavelength, λ_{em}, of R01 compound (465 nm) is strongly agrees with the experimental results (467 nm) (Wang

et al., 2015), supporting our selection of the theoretical level of calculation. Comparing with the parent molecule (R01), the majority of the new designed molecules show a red shift in the emission spectrum, whereas some of them show a blue shift, with a significant increase in the oscillator strength as in the case of molecules D5, D6 and D7. The highest oscillator strength is found for D5. In addition, the emission spectra show a blue shift in the order D4 (λ_{em} = 453 nm) → T9 (454 nm) = D1 (λ_{em} = 454 nm) → H12 (460 nm). On the other hand, the emission spectra show a red shift in the order T8 (λ_{em} = 468 nm) → D2 (λ_{em} = 476 nm) = T11 (483 nm) → D7 (490 nm) = D6 (490 nm) → D3 (498 nm) → T10 (503 nm) → D5 (504 nm). Generally, for the parent and designed derivatives, the emission maxima are longer than the absorption maxima, since λ_{em} is red-shifted by not less than 52 nm compared with λ_{abs}.

3.7. Stokes shift

Stokes shift can reflect the degree of structural deformation between the ground state and excited state geometries. A more substantial Stokes shift is beneficial for pore-filling of HTM (Chi et al., 2016). The computed results of the newly designed molecules yield a stoke shift values (λ_{ss}), described as: $\lambda_{ss} = \lambda_{em} - \lambda_{abs}$. Based on the values of the calculated λ_{ss} (Table 4), the new designed compounds can be classified into three categories as follows:

(a) Relatively high λ_{ss} (from 106 nm to 119 nm) (D6, T8, T9, T8 and T11 compounds): The relatively high λ_{ss} values indicate that electron transition breaks the strong conjugative effect and leading to a remarkable geometry distortion (bond lengths and bond angles (Table 1). and large reorganization energy as will be shown in the next subsection (Table 5).
(b) Relatively moderate λ_{ss} (from 84 nm to 105 nm) (D3, D2, D5, H12 and D7 compounds). The moderate λ_{ss} value reflects that electron transition is partially breaking the strong conjugative effect, which leads to a moderate geometry distortion from a ground state to an excited state and a moderate reorganization energies (Table 1 and Table 5).

Table 5 Internal hole λ_{hole}/electron λ_{elec}/total λ_{tot} reorganization energies along with their components, $\lambda_1, \lambda_2, \lambda_3$ and λ_4, the adiabatic and vertical ionization potentials, electron affinities, hole/electron extraction potentials, and global hardness η (in eV) of investigated HTMs calculated at the B3LYP/6-31G(d).

HTM	λ_1	λ_2	λ_{hole}	λ_3	λ_4	λ_{elec}	λ_{tot}	IP_a	IP_v	HEP	EA_a	EA_v	EEP	η
R01	0.141	0.156	0.297	0.161	0.207	0.368	0.665	5.751	5.907	0.206	0.462	0.255	0.023	2.645
D1	0.177	0.198	0.374	0.163	0.175	0.338	0.712	5.673	5.871	0.202	0.360	0.185	0.019	2.656
D2	0.158	0.155	0.313	0.207	0.202	0.410	0.723	5.642	5.797	0.202	0.119	−0.083	0.012	2.761
D3	0.135	0.145	0.280	0.181	0.237	0.418	0.698	5.631	5.776	0.202	0.431	0.194	0.022	2.600
D4	0.149	0.164	0.313	0.203	0.232	0.435	0.748	5.621	5.785	0.201	0.277	0.044	0.018	2.672
D5	0.134	0.131	0.264	0.167	0.213	0.380	0.645	5.662	5.792	0.203	0.464	0.251	0.023	2.599
D6	0.067	0.347	0.415	0.210	0.230	0.441	0.855	5.565	5.912	0.202	0.366	0.135	0.021	2.600
D7	0.067	0.354	0.421	0.205	0.228	0.433	0.854	5.560	5.914	0.202	0.366	0.138	0.021	2.597
T8	0.080	0.072	0.152	0.270	0.247	0.517	0.669	6.066	6.138	0.220	0.203	−0.044	0.017	2.931
T9	0.031	0.633	0.664	0.200	0.209	0.409	1.073	5.529	6.163	0.202	0.155	−0.054	0.013	2.687
T10	0.155	0.164	0.319	0.182	0.197	0.380	0.699	5.549	5.713	0.198	0.325	0.128	0.019	2.612
T11	−0.041	0.501	0.460	0.249	0.235	0.484	0.944	5.396	5.897	0.200	0.267	0.032	0.019	2.564
H12	0.210	0.154	0.365	0.221	0.215	0.436	0.800	5.824	5.978	0.206	0.117	−0.099	0.012	2.854

(c) Relatively small λ_{ss} (52–80 nm) (R01, D1 and D4 compounds), which indicates that electron transition doesn't break the strong conjugative effect, assigning a small geometry distortion and a small reorganization energies (Table 1 and Table 5).

Since larger Stokes shift is also typical feature for a good HTM; we could predict that D6, T8, T9, and P9 derivatives as HTMs are better for increasing the performance of PSCs compared with the parent (R01). D6 and T8 combine in the nature of the methoxy position, the two and four methoxy groups in D6 and T8, respectively, are positioning in the ortho- and meta- positions. In D6, the methoxy groups are in o1m7, and in T8 they are in o1o2m3m4, see Scheme 1. While the four methoxy groups in T9 are at the four *ortho*-positions (o1o2o5o6).

3.8. The radiative lifetimes

The Radiative lifetimes (τ) of the compounds under probe have been computed for a spontaneous emission using the Einstein transition probabilities (Lukeš et al., 2005). This time refers to the average time that molecules stay in their excited state before emitting a photon. If the compounds have a shorter lifetime in the excited state, it means they have more efficiency in the emitting of fluorescence or photons (Zhang et al., 2012a, 2012b), and longer lifetime indicate improved suppression of back reactions of the injected electrons, this results in improvement the V_{oc} value, due to the reduced electron recombination rate (Kim et al., 2015). The calculate lifetime τ for the investigated compounds are listed in Table 4. It was pointed that the shorter radiative lifetimes, the high light-emitting efficiency, while the longer radiative lifetime facilitates the electron and energy transfer (Hlel et al., 2015). According to Table 4, it has been observed that as the radiative lifetime of compounds is shortened, the oscillator strength is increased. These results lead to an increase in the luminescent efficiency. The computed τ values follow the following order: H12 > D4

> D2 > T10 > D3 > T9 > T11 > T8 > D1 > D7 > R01 > D5 > D6. For compound H12, with six methoxy groups, we find the lowest oscillator strength and the longest radiative lifetime, whereas the shortest radiative lifetime and the highest oscillator strength is found for compounds D5 and D6, with only two substituted methoxy groups. Therefore, they should be good-emitting materials with a high efficiency (Zhang et al., 2012a, 2012b).

To better explain the contribution of the electron, the charge density differences between ground and excited states of R01 and some of its designed derivatives, D1, D2, T9, T11, and H12 (as representative examples) are plotted in Table 6. In this case, it is assumed to be the difference between HOMO and LUMO since the first transition is mainly from HOMO to LUMO. Electron density moves from the cyan region to the blue region when moving from the ground state to the first excited state. Cyan and blue colors indicate increase and decrease of charge densities, respectively. As evident from Table 6 the R01 and its derivatives demonstrated clearly intramolecular charge transfer (ICT).

3.9. Reorganization energy, electron affinity, and ionization potential

One of the parameters to determine the carrier hopping rate is the reorganization energy ($\lambda\lambda$), which comes from the contributions of external reorganization energy and internal reorganization energy. The latter includes the molecular geometry modifications when an electron is added or removed from a molecule, and the former is the modifications in the surrounding medium due to polarization effects. Norton and Brédas (Norton and Brédas, 2008) reported that the external reorganization energy is significantly lower than that of the inner part based on a polarized force field calculation. It is also fundamental to calculate the ionization potential (*IP*) and electron affinity (*EA*), which characterize the reduction and oxidation properties (Chen et al., 2011). These descriptors can be used to evaluate the energy barriers of holes and electron injection

Table 6 Density difference between ground state (S_o) and excited state (S_1) of some investigated HTMs (as representative examples), contour threshold is 0.02 au.

HTM	ED moves from S_o	ED goes to S_1	Full picture
R01			
D1			
T11			
H12			

including charge mobility and balanced charge. The calculated adiabatic and vertical IPs (IP_a and IP_v), the adiabatic and vertical EAs (EA_a and EA_v), as well as the reorganization energies for holes ($\lambda\lambda_{hole}$) and electrons ($\lambda\lambda_{elec}$) for the compounds under probe at B3LYP/6-31G(d) are presented in Table 5 and Fig. 4 Also, Table 5 includes the values of HEP (the hole extraction potential) as the energy difference from M^+ (cationic) to M (neutral molecule), using M^+ geometric structure in the calculation, and EEP (the electron extraction potential) as the energy difference from M- (anionic) to M, using M- geometric structure in the calculation (Chen et al., 2014a, 2014b). The internal reorganization energy is the energy difference between two molecules due to geometric relaxation during electron transfer, and it is an important parameter for charge transfer and according Marcus theory (Nelsen et al., 2001), which provides to a qualitative indication of the charge-transport rate (the lower the λ values, the bigger the charge-transport rate). For reorganization energy, as is seen in Table 5, the $\lambda\lambda_{hole}$ values of the investigated molecules are ranged from 0.152 to 0.664 eV, while the λ_{elec} values are in the interval of 0.338–0.517 eV. As shown, the first important remark to be noted is that most of the investigated molecules exhibit λ_{elec} values larger than the λ_{hole} values, except of D1D1 and T9, implying that the hole transfer should be faster than the electron transport, which is reflected by the k_{hole} and k_{elec} values (1.03 × 10^{14}–1.86 × 10^{15}, and 4.91 × 10^{14}–6.79 × 10^{15} s^{-1}, respectively). From the variations in the main geometrical parameters in the neutral to anionic/cationic states, see Section 3.1, we observed that the geometry relaxation between the neutral and anion states is greater than that for the cations, resulting in

greater polarization in the former, which results in a larger value of λ_{elec} than λ_{hole} (Irfan et al., 2015).

We find that the λ_{hole} of the parent molecule, R01 is only 0.297 eV, while its λ_{elec} reaches as high as 0.368 eV; the latter is higher than the former. Hence, R01 should be suit to transporting holes than electrons. These results indicate, from the reorganization energy point of view, that R01 is p-channel rather than n-channel. In addition, the λ_{hole} of R01 is approximately equal to that of a typical hole transport material N, N′-diphenyl-N,N′-bis(3-methylphenyl)-(1,1 0-biphenyl)-4,4′-diamine (TPD) with λ_{hole} = 0.29 eV. This also means that its hole transfer rate, (k_{hole} = 1.9 × 10^{15} s^{-1}), should be approximately equal that of TPD, thus the potential of R01 compound as tested experimentally as profound hole transfer material, is also proved theoretically. Unlike the others, T9 and T11 displayed considerable hole reorganization energies (0.664 eV and 0.460 eV, respectively), which can be ascribed to their large structural distortions when the ionization process takes place (Table 1). In comparison with the parent molecule (R01), most R01 derivatives exhibit larger λ_{hole} and λ_{elec} values, except D3, D5 T8 and T8 D5exhibit smaller λ_{hole} value and only D1 exhibits smaller λ_{elec} value. These results indicate that most of the designed derivatives may possess lower charge mobilities compared to that of the parent, which can be easily noticed from the k_{hole} values. On the other hand, the calculated λ_{hole} values for D3, D5 T8 and T8 D5are 0.280, 0.152 and 0.264 eV, respectively, which are clearly smaller than that of the value of R01 (0.297 eV). D3T8D5, indicating that these designed HTMs have larger hole mobilities compared to the parent. While, D1 with λ_{elec} (0.338 eV) which is smaller than
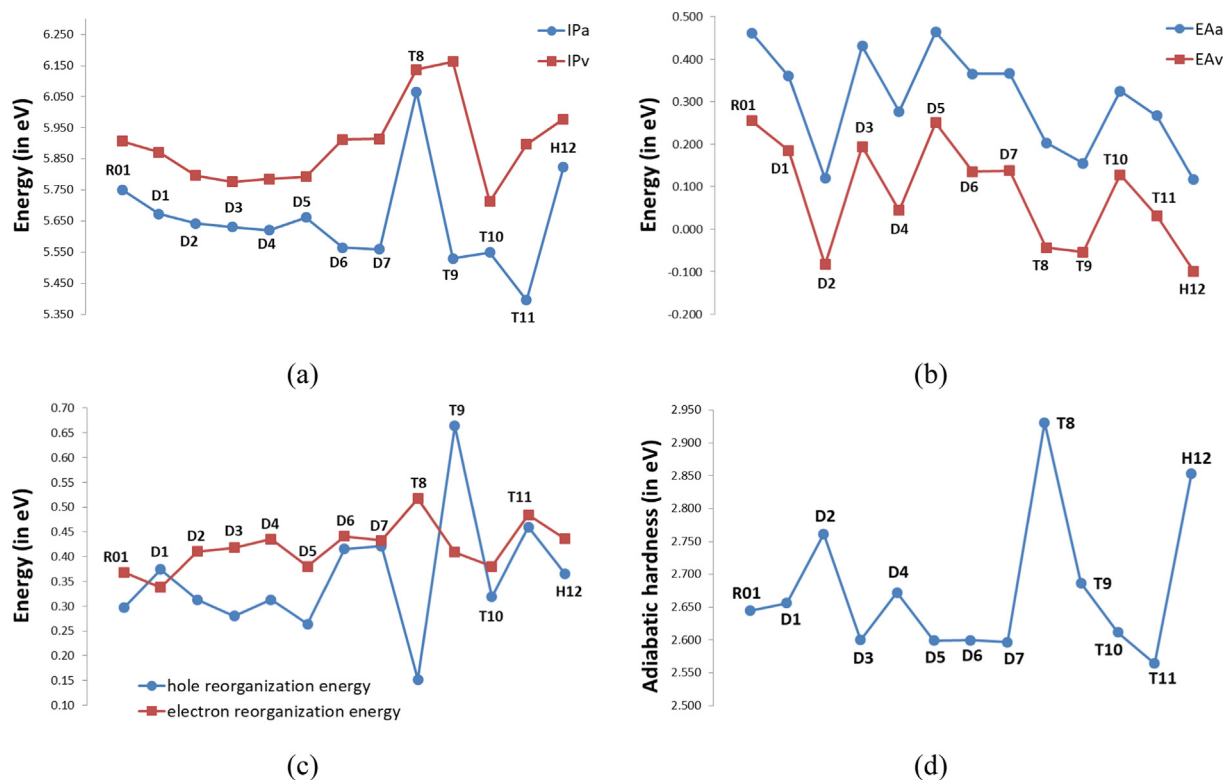
Fig. 4 Adiabatic and vertical ionization potentials (IP_v/IP_a), (b) Adiabatic and vertical electronic affinities (EA_v/EA_a), (c) hole reorganization energies (λ_{hole}) and electron reorganization energies (λ_{elec}), and (d) adiabatic hardness of investigated HTMs calculated at the B3LYP/6-31G(d).

that of R01 (0.368 eV), clearly demonstrating that this compound has larger electron mobility compared to that of the parent. The trend of increasing of the λ_{hole} values of the di-methoxy derivatives is D5 < D2 = D4 < D3 < P1 < D6 < D7, thus among this series, D5 is expected to show the faster hole transfer. While, for the series composed of the tetra-methoxy derivatives the trend observed is: T8 < T10 < T11 < T9, and in this series T8 and T9 are the compounds that expect to show the faster and slower hole transfer, respectively. On the other hand, the trend of increasing of the λ_{elec} values of the di-methoxy derivatives is D1 < D5 > D2 < D3 < D7 < D4 < D6, thus among this series, D1 and D6 are expected to show the faster and slower electron transfer, respectively. While, for the series composed of the tetra-methoxy derivatives the trend observed is: T10 < T9 < T11 < T8, and in this series T10 and T8 are the compounds which expect to show the faster and slower hole transfer, respectively. However, H12 the *hexa*-methoxy derivative has intermediate hole and electron mobilities. In order to attain high quantum efficiency, it is necessary to achieve efficient charge injection at right charge balance; thus, materials used as hole/electron transporter should have closed reorganization energy with bipolar character (Chen et al., 2014a, 2014b). Therefore, most of the designed derivatives (except five out of twelve compounds, *i.e.,* D3, D4, D5, T8, and T9), have comparable/better potential as HTMs as R01, since the difference between the λ_{hole} and λ_{elec} is only in the range 0.012 to 0.097 eV, while the difference for the parent is 0.072 eV.

To compare the magnitudes of hole and electron mobilities, we calculate the relative hopping rates of holes versus electrons, k_{elec}/k_{hole}. The values of k_{hole} and k_{elec} have been calculated, assuming T to be 300 K and neglecting the difference in ΔH_{ab}, (Table 7). The ratio is predicted to be in the range 2–30. Where most of the investigated molecules show small ratio (between 2 and 6), where D6, D7 and H12 show relatively large ratio (30, 22, 22, respectively), and P2, D5, and T9 show moderate values, 18, 13, and 15, respectively. Although some experimental data indicated that ΔH_{ab} varies over a rather limited range for intramolecular charge-transfer processes, this does not guarantee complete cancellation in the comparison of relative charge-transfer rates. The hole mobility of R01 has been reported to be 2.05×10^{-4} cm^2 V^{-1} s^{-1} (Wang et al., 2015). However, direct comparison of its reported mobility is not feasible because the value depends on the electric field and film preparation details.

As is known the ionization potential and electron affinity are good descriptors to interpret the charge transfer behavior. The energy barrier for the injection of holes and electrons can be predicted by the explicit properties such as adiabatic ionization potential (IP_a) and adiabatic electron affinity (EA_a). Evaluation of the nature of devices of carrier transport can be measured by the stability of the HTMs. The stability of p-type HTMs is directly related to the IP_a. The lower ionization potential indicates that material would be better as hole transporter, while higher electron affinity leads to be a better electron transport (Chan and Liao, 1970). The adiabatic ionization potential (IP_a), vertical ionization potential (IP_v), adiabatic electron affinity (EA_a), and vertical electron affinity (EA_v) were calculated. The computed results are summarized in Table 5. The trend observed for the change in the adiabatic and vertical EA values of the investigated HTMs is very similar. In contrast, there is a small difference between the trend of changes showed by the adiabatic and vertical IP values, as illustrated in Fig. 4. Additionally, for all investigated HTMs, the adiabatic IP values are smaller than the vertical IP values, while the reverse is true with respect to the EA values.

The data in Table 5 and Fig. 4 shows that the order of decreasing the adiabatic and vertical EA values of the di-methoxy derivatives with respect to that of the parent is: R01 > D5 > D3 > D6 ≈D7 > P1 > D4 > P2, while that for the tetra-methoxy HTMs is: R01 > T10 > P9 > T8 > T9, and the EA values of R01 are larger than that of the *hexa*-methoxy (H12) derivative. Thus, the parent compound show higher EA values compared to those of its derivatives, indicating that R01 seems to be a better electron transporting material than its methoxy-substituted derivatives. In addition, D2, T8, T9, and H12 derivatives have negative calculated EA_v values, different from others, which was raised by the incomplete cancellation of the electronic self-interaction energy due to the use of an inexact density functional and a finite basis set (Chen et al., 2014a, 2014b). The four aforementioned HTMs are expected to show the weakest potential as electron transporting materials. However, from the adiabatic/vertical EA values of D1 (0.360/0.185 eV), D3 (0.431/0.194 eV), and D5 (0.464/0.251 eV), these three di-methoxy derivatives are expected to show comparable potential as that of the parent

Table 7 Calculated change transfer integrals, (t_{hole} and t_{elec} (in eV), hopping rate constants, (k_{hole} and k_{elec} (in s^{-1}), and the relative hopping rate for the investigated HTMs calculated at the B3LYP/6-31G(d) level.

HTM	t_{hole}	t_{elec}	k_{hole}	k_{elec}	k_{elec}/k_{hole}
R01	0.246	0.391	1.86×10^{15}	4.22×10^{15}	2
D1	0.218	0.365	1.30×10^{15}	3.82×10^{15}	3
D2	0.114	0.161	3.88×10^{14}	6.79×10^{15}	18
D3	0.205	0.451	1.34×10^{15}	5.26×10^{15}	4
D4	0.162	0.273	7.93×10^{14}	1.88×10^{15}	2
D5	0.095	0.377	2.96×10^{14}	3.86×10^{15}	13
D6	0.047	0.262	5.79×10^{13}	1.73×10^{15}	30
D7	0.057	0.266	8.39×10^{13}	1.81×10^{15}	22
T8	0.094	0.192	3.82×10^{14}	8.55×10^{14}	2
T9	0.033	0.113	2.22×10^{13}	3.32×10^{14}	15
T10	0.176	0.394	9.21×10^{14}	4.23×10^{15}	5
T11	0.001	0.167	1.03×10^{14}	6.69×10^{14}	6
H12	0.028	0.139	2.24×10^{13}	4.91×10^{14}	22

(0.462/0.255 eV). On the other hand, the adiabatic and vertical *IP* values of all designed methoxy derivatives are smaller than that of the parent (except those of D6, T8, T9, and H12), indicating that most of the designed HTMs are seemed to be better hole transporting materials than the parent compound. Both the values of the adiabatic/vertical *IP* of T8 (6.066/6.138 eV) and H12 (5.824/5.978 eV) are larger than that of R01 (5.751, 5.907 eV), indicating that these tetra- and *hexa*-methoxy derivatives, respectively, and relying on these values only are the least potential designed molecules as hole-transporting materials. The first inspection of Table 5 shows that T11 has the lowest IP_a (5.395 eV) and its EA_a (0.267 eV) is considered as a medium value as compared with other eleven molecules. However, the parent compound R01 has the highest EA_a (0.462 eV) and its IP_a is relatively high (5.751 eV) compared to its derivatives. We can also find that molecule T8 (6.066 eV) has the biggest IP_a value and a relatively small EA_a value (0.267 eV). Importantly, our computed results show that IP_a is higher when 4 and /or six methoxy groups have been introduced to the parent molecules. On the other hand, the biggest EA_a value is reported for D5 (0.464 eV) while the smallest EA_a value is found for H12 (0.115 eV) as compared with the other molecules. The vertical *IP* and *EA* values calculated at the geometry of the neutral molecule can be used to study the charge injection of the materials. The molecule with low *IP* or high *EA* is likely to improve electron or hole

injection/transport (Chen et al., 2014a, 2014b). It can be found that the change trends of the vertical *IP* and *EA* values for the investigated HTMs are almost similar to their HOMO and LUMO energies. The correlation between IP_v values and HOMO energies (EA_v values and LUMO energies) for the HTMs with di-methoxy substitution and tetra-methoxy substitution all with the parent can be obtained linearly in Fig. 5.

Di-methoxy derivatives (D1, D2, D3, D4, D5, D6, and D7); along with R01

$$IP_v = 1.0917(-E_{HOMO}) + 0.6438; \quad R^2 = 0.9085$$

$$EA_v = 0.9020(-E_{LUMO}) + 0.7334; \quad R^2 = 0.9682$$

Tetra-methoxy derivatives (T8, T9, T10, and T11); along with R01

$$IP_v = 1.101(-E_{HOMO}) + 0.5976; \quad R^2 = 0.8366$$

$$EA_v = 0.7621(-E_{LUMO}) + 0.5663; \quad R^2 = 0.9711$$

Above regression equations may provide a simple formula to predict the vertical *IP* and *EA* values of other similar derivatives from their HOMO and LUMO energies (Zhang et al., 2012a, 2012b; Chen et al., 2014a, 2014b). Previous studies have demonstrated that the IP_a values of air-stable p-channel materials ranges from 5.680 eV to 6.786 eV, and the EA_a values for air-stable n-channel ones are in the range 2.411 to 3.141 eV

(a)

(b)
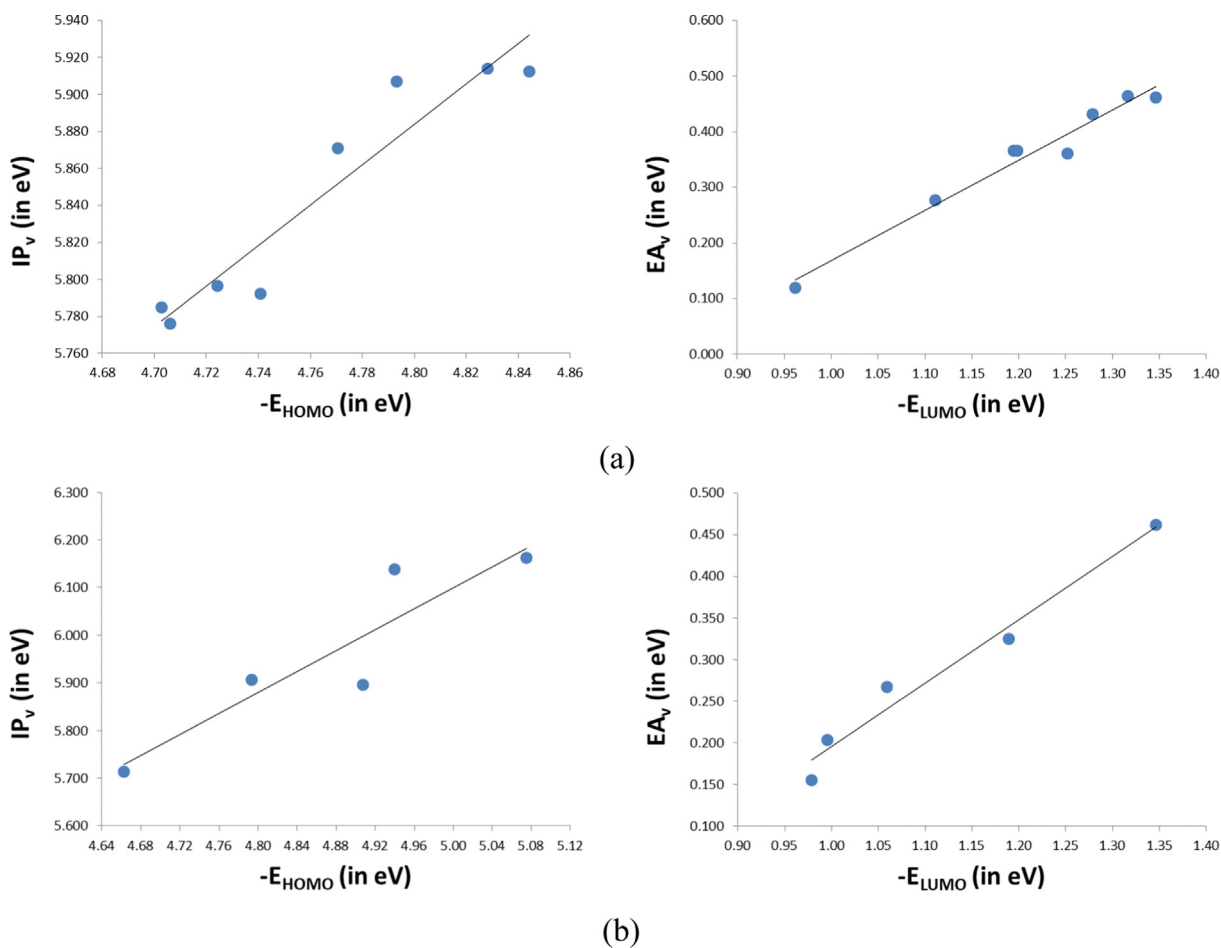
Fig. 5 The correlation between the calculated HOMO and LUMO energies and the vertical *IP* and *EA* values in (a) Di-methoxy derivatives and (b) Tetra-methoxy derivatives.

(Zhao et al., 2013). On the basis of this viewpoint, only R01, T8, and H12 should be air-stable p-channel materials, while non-compound is an air-stable n-channel one. Hence, the investigated HTMs are not suitable to being used as electron transport materials for their low air-stability.

Furthermore, the absolute hardness (η) also has been calculated. As is known, hardness (η) is the resistance of the chemical potential to the change in the number of electrons, and it's controlled the stability of PSC, since the HTM could play a crucial role in controlling the stability of PSCs; an ideal HTM should be stable, *i.e.*, it should be a hard molecule with large η value (Zhang et al., 2017a, 2017b). The η values of all molecules are also presented in Table 5 and Fig. 4. Inspection of Table 5 and Fig. 4 reveals that the η values of the designed molecules in the range 2.564–2.931 eV with largest deviation of 0.37 eV, indicating that the stabilities of the investigated molecules are almost similar. Indeed, we have found that T8 ($\eta = 2.931$ eV) molecule has the highest stability while T11($\eta = 2.564$ eV) molecule has the lowest stability among all the studied molecules. The previous result indicates that the stability of R01 derivatives is comparable to that of Spiro-OMeTAD and ATT derivatives (Chi et al., 2016).

3.10. First singlet excitation and exciton binding energies

As is known the exciton binding energy (E_b) of samples is an important factor for the electroluminescence quantum efficiency of organic light-emitting diodes (OLEDs) (Franceschetti and Zunger, 1997; Cao et al., 1999). The computed First singlet excitation and excitation binding energies are presented in Table 3. As shown in Table 3, the investigated molecules have large exciton binding energy in the range 0.357–0.571 eV (Hlel et al., 2015). The molecule D5 (0.357 eV) has the lowest E_b and molecule H12 (0.571 eV). Our results show that the calculated $E_b \geq k_B T$ 0.331eV at room temperature, reflecting that the investigated molecules certainly allow the formation of exciton even at room temperature after excitation and leading to higher fluorescence quantum efficiency after recombination in OLEDs (Hlel et al., 2015).

3.11. NLO properties

It has found that compounds with nonlinear optical properties have good photoelectric conversion performance (Cai-Rong et al., 2009; Kumar et al., 2010; Garza et al., 2014). The polarizabilities and hyperpolarizabilities of the six investigated HTMs were calculated at the B3LYP/6-311 + +G(d,p), Fig. 6. In addition to the total hyperpolarizabilities, the isotropic polarizability, polarizability anisotropy invariant and hyperpolarizability.

The calculated isotropic polarizability ($\Delta\alpha$) values of D1-D7, T9-T11, and H12 are in the range from 397-to-647 au However, the calculated isotropic polarizability of the parent molecule R01 is an intermediate value ($\Delta\alpha = 568au$) compared to those of its derivatives. The isotropic polarizability values of the designed D1 and D3 are very comparable to that of the R01 (the parent molecule), therefore, the specific positions of the substituent methoxy groups in these two designed HTMs make them with comparable response to the external electric field compared to R01. The designed H12 shows the least value (397 au). As reported an inverse correlation was found between the isotropic polarizability values and photo-to-current conversion efficiencies, and this was attributed to the fact that larger delocalization of electrons enhanced the response to the external field, but it is less efficient in generating charge separated state (Cai-Rong et al., 2009). Thus, it induced the lower photo-to-current conversion efficiency. According to the values of the isotropic polarizability, the efficiencies of the investigated HTMs to convert photons into electricity can be estimated as: D5 (647 au) > R01 (568 au) > D3 (562 au) > D1 (557 au) > T10 (543 au) > D7 (528 au) ≥ D6 (525 au) > T11 (500 au) > D4 (484 au) > D2 (420 au) > T8 (414 au) > T9 (406 au) > H12 (397 au).

As shown in Fig. 6, the order of decreasing the total hyperpolarizabilities (β_{tot}) of the investigated di-methoxy HTMs in comparison with R01 is: D5 (1420 au) > D4 (1399 au) > D2 (1324 au) > D6 (919 au) > D7 (866 au) > R01 (700 au) > D1 (644 au) ≫ D3 (174 au). The order of decreasing the total hyperpolarizabilities of the investigated tetra-methoxy HTMs in comparison with R01 is: T11 (959 au) > R01 (700 au) > T8 (587 au) ≫ T9 (256 au) ≫ T10 (32 au). In contrast, the hyperpolarizability of the parent (R01) is seven times greater than that of the *hexa*-methoxy derivative H12 (96 au). Generally, the di-methoxy derivatives have the largest hyperpolarizabilities (except D3), ranges from 1420-to-644 au, followed by the tetra-methoxy derivatives (except T10), ranges from 959-to-256 au, and then the H12 with six methoxy substituents has the least hyperpolarizability. Indeed, the major
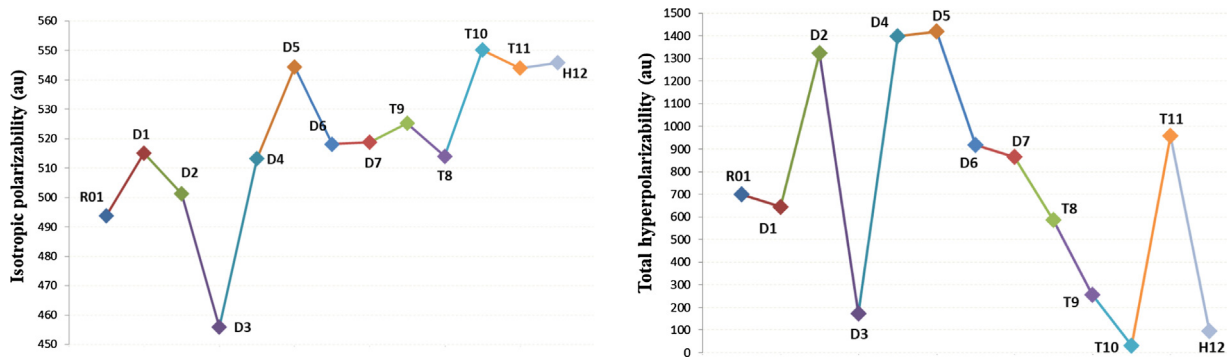
Fig. 6 Isotropic polarizability and total hyperpolarizability values (in au) of investigated HTMs calculated at the B3LYP/6-311 + +G(d, p).

factor affecting the hyperpolarizability values is the number of methoxy groups (as the number of the methoxy groups increasing, the hyperpolarizability decreasing), while their positions seems to has a minor effect on the hyperpolarizability values. The total hyperpolarizabilities for R01 molecule is 700 au, which is smaller than that of the typical NLO material *p*-nitroaniline (pNA) ($\beta_{tot} = 1327au$) that has been calculated at B3LYP/6-31G(d,p) (Garza et al., 2014). D2 and D4 are found to have considerably larger hyperpolarizabilities compared to the parent molecule and very comparable values compared to pNA, and D4 shows even larger value by ∼72 au. The difference between the four designed HTMs D1-D4 is in the position of the substituted methoxy groups, since all of these molecules have two substituted methoxy groups at different positions in the carbazole rings. From the data above, it is possible to conclude that the specific positions of the methoxy groups is believed to contribute with different extent to electron donor ability to the CT, hence leading to different hyperpolarizability. It is interested to note that, H12 molecule shows the very small value of total hyperpolarizability equals 96 au. Thus, the substitution of the six hydrogen atoms with methoxy results in a remarkable decrease in the molecule's total hyperpolarizability. As previously mentioned, the methoxy substituent has an electron-donating ability through resonance and electron-withdrawing ability inductively; it seems that when the number of methoxy groups becomes six (as in H12) the second effect becomes more pronounced, leading to lesser electron donor ability to the CT and smaller.

4. Conclusion

In this report, an investigation on twelve new designed molecules by means of DFT and TD-DFT methods has been performed. The designed molecules are derivatives of the well experimentally tested R01 used as a hole transporting material for perovskite solar cell applications. R01 is a carbazole-based compound. The designed derivatives differ in number (two, four, and six) and positions of methoxy groups (*ortho*- and *meta*-) with respect to the dioxythiophene ring, resulting in the different effect of the substituted methoxy groups with various electronic structures and optoelectronic properties of the designed HTMs. The most important concluded remarks from this report are:

1. In most cases, the number and position of the substituted methoxy groups have a major effect on geometrical parameters of the ground states. The most affected parameter is the $S-C-C-C$ dihedral angles those represent the extent of planarity of the molecule. As expected, the tetra- and *hexa*-methoxy derivatives showed the most significant changes, due to the steric hindrance of the methoxy groups.
2. Due to methoxy substitution, the HOMO energy levels of most designed HTMs are stabilized and become more close to that of the valence band of perovskite than that of R01, which is beneficial to improving the V_{oc}. In contrast, the LUMO energy levels of all designed molecules are destabilized and become higher than that of the conduction band of perovskite to efficiently block the electron recombination. This is because, the substituted methoxy groups contributing in larger extent to HOMOs compared to their contribution to the LUMO.

3. The investigated HTMs show a dominant ICT that demonstrated by the π-π* that dominated for R01 and most of its derivatives by HOMO-LUMO transition and from the charge density differences between ground and excited states.
4. In comparison to the R01, as the number of substituted methoxy groups increases, the maximum absorption wavelengths would be blue shifted, whereas, the introduction of two methoxy groups keeps the λ_{abs} in the visible region.
5. The linear relationships between the vertical *IP* and *EA* values for the investigated HTMs with their HOMO and LUMO energies ($R^2 = 0.837 - 0.971$) may provide a simple formula to predict those values of other similar derivatives from their HOMO and LUMO energies.
6. The hole reorganization energies of most investigated HTMs including the parent molecule (R01) are smaller than their electron reorganization energies, indicating that these compounds will efficient hole transporting materials, while D1 and T9 derivatives would expect to be effective as electron transporting materials, because their hole reorganization energies are more significant than their electron reorganization energies.
7. The higher Stokes shift values from absorption to emission of D6, T8, T9, and T11 compounds showed that these derivatives would be efficient materials for multipurpose semiconductor applications.
8. NLO parameters calculations showed that β_{tot} values of D5, D4 are very comparable (larger by ∼48 and ∼27 au, respectively), to that of the typical NLO material pNA, indicating their potential for NLO applications. On the other hand, T10, H12, and D3 show the least potential as NLO materials, their β_{tot} values are significantly small (32, 96, and 174, respectively) and much lower compared to that of pNA. The β_{tot} value of pNA is 43, 14, and 8 times greater than those of the aforementioned HTMs, respectively. In general, the R01 and other derivatives show moderate potentials as NLO materials when comparing their β_{tot} values with that of pNA.

It is not the sole and determined item to affect the overall performance. In view of suitable frontier molecular orbital, larger Stokes shift and high hole mobility and other factors, the designed molecules as HTMs can act as a promising candidate. We believe that this study shed light on the effect of methoxy groups on the electronic and photophysical properties of carbazole-based HTMs, with molecular level insight using the quantum chemical calculations, the methoxy derivatives of R01 may be candidates for optoelectronic materials application and worthy of experimental investigations.

References

Ansari, M.I.H., Qurashi, A., Nazeeruddin, M.K., 2018. Frontiers, opportunities, and challenges in perovskite solar cells: a critical review. J. Photochem. Photobiol., C 35, 1–24.

Bagheri Novir, S., Hashemianzadeh, S.M., 2015. Density functional theory study of new azo dyes with different π-spacers for dye-sensitized solar cells. Spectrochim. Acta Part A: Mol. Biomol. Spectrosc. 143, 20–34.

Baryshnikov, G., Minaev, B.F., Minaeva, V., Ning, Z., Zhang, Q., 2012. Structure and spectral properties of truxene dye S5. Opt. Spectrosc. 112 (2), 168–174.

Becke, A.D., 1988. Density-functional exchange-energy approximation with correct asymptotic behavior. Phys. Rev. A 38 (6), 3098–3100.

Bi, D., Tress, W., Dar, M.I., Gao, P., Luo, J., Renevier, C., Schenk, K., Abate, A., Giordano, F., Baena, J.-P.C., 2016. Efficient luminescent solar cells based on tailored mixed-cation perovskites. Science advances 2 (1), e1501170.

Cai-Rong, Z., Zi-Jiang, L., Yu-Hong, C., Hong-Shan, C., You-Zhi, W., Li-Hua, Y., 2009. DFT and TDDFT study on organic dye sensitizers D5, DST and DSS for solar cells. J. Mol. Struct. (Thoechem.) 899 (1–3), 86–93.

Cai, F., Cai, J., Yang, L., Li, W., Gurney, R.S., Yi, H., Iraqi, A., Liu, D., Wang, T., 2017. Molecular engineering of conjugated polymers for efficient hole transport and defect passivation in perovskite solar cells. Nano Energy.

Calió, L., Kazim, S., Grätzel, M., Ahmad, S., 2016. Hole-transport materials for perovskite solar cells. Angew. Chem. Int. Ed. 55 (47), 14522–14545.

Cao, Y., Parker, I.D., Yu, G., Zhang, C., Heeger, A.J., 1999. Improved quantum efficiency for electroluminescence in semiconducting polymers. Nature 397 (6718), 414.

Chan, R., Liao, S., 1970. Dipole moments, charge-transfer parameters, and ionization potentials of the methyl-substituted benzene–tetracyanoethylene complexes. Can. J. Chem. 48 (2), 299–305.

Chen, X.-K., Zou, L.-Y., Huang, S., Min, C.-G., Ren, A.-M., Feng, J.-K., Sun, C.-C., 2011. Theoretical investigation of charge injection and transport properties of novel organic semiconductor materials—cyclic oligothiophenes. Org. Electron. 12 (7), 1198–1210.

Chen, X., Jia, C., Wan, Z., Zhang, J., Yao, X., 2014a. Theoretical investigation of phenothiazine–triphenylamine-based organic dyes with different π spacers for dye-sensitized solar cells. Spectrochim. Acta Part A: Mol. Biomol. Spectrosc. 123, 282–289.

Chen, X., Kong, C.-P., Bai, F.-Q., Zhang, H.-X., 2014b. Theoretical study on the electronic structures and properties of diindolocarbazole isomers. J. Phys. Org. Chem. 27 (12), 973–980.

Chi, W.-J., Li, Z.-S., 2015a. The theoretical investigation on the 4-(4-phenyl-4-[small alpha]-naphthylbutadieny)-triphenylamine derivatives as hole transporting materials for perovskite-type solar cells. PCCP 17 (8), 5991–5998.

Chi, W.-J., Li, Z.-S., 2015b. The theoretical investigation on the 4-(4-phenyl-4-α-naphthylbutadieny)-triphenylamine derivatives as hole transporting materials for perovskite-type solar cells. PCCP 17 (8), 5991–5998.

Chi, W.-J., Sun, P.-P., Li, Z.-S., 2016. A strategy to improve the efficiency of hole transporting materials: introduction of a highly symmetrical core. Nanoscale 8 (41), 17752–17756.

Chitpakdee, C., Namuangruk, S., Khongpracha, P., Jungsuttiwong, S., Tarsang, R., Sudyoadsuk, T., Promarak, V., 2014. Theoretical studies on electronic structures and photophysical properties of anthracene derivatives as hole-transporting materials for OLEDs. Spectrochim. Acta Part A: Mol. Biomol. Spectrosc. 125, 36–45.

Franceschetti, A., Zunger, A., 1997. Direct pseudopotential calculation of exciton coulomb and exchange energies in semiconductor quantum dots. Phys. Rev. Lett. 78 (5), 915.

Gao, H.-Z., 2010. Theoretical studies of electronic structure and hole drift mobility of host hole transporting material 4,4′-N, N′-dicarbazol-biphenyl. Synth. Met. 160 (19–20), 2104–2108.

Garza, A.J., Wazzan, N.A., Asiri, A.M., Scuseria, G.E., 2014. Can Short- and middle-range hybrids describe the hyperpolarizabilities of long-range charge-transfer compounds? J. Phys. Chem. A 118 (50), 11787–11796.

Gorelsky, S.I., 2015. Program for Molecular Orbital Analysis.

Gorelsky, S.I., Lever, A.B.P., 2001. J. Organomet. Chem. 635, 187–196.

Green, M.A., Ho-Baillie, A., Snaith, H.J., 2014. The emergence of perovskite solar cells. Nat. Photonics 8 (7), 506–514.

Grigalevicius, S., Ma, L., Grazulevicius, J.V., Xie, Z.-Y., 2006. Well defined carbazole-based hole-transporting amorphous molecular materials. Synthetic Metals 156 (1), 46–50.

Hlel, A., Mabrouk, A., Chemek, M., Khalifa, I.B., Alimi, K., 2015. A DFT study of charge-transfer and opto-electronic properties of some new materials involving carbazole units. Comput. Condens. Matter 3, 30–40.

Igbari, F., Li, M., Hu, Y., Wang, Z.-K., Liao, L.-S., 2016. A room-temperature CuAlO$_2$ hole interfacial layer for efficient and stable planar perovskite solar cells. J. Mater. Chem. A 4 (4), 1326–1335.

Irfan, A., Al-Sehemi, A.G., Muhammad, S., Chaudhry, A.R., Al-Assiri, M.S., Jin, R., Kalam, A., Shkir, M., Asiri, A.M., 2015. In-depth quantum chemical investigation of electro-optical and charge-transport properties of trans-3-(3,4-dimethoxyphenyl)-2-(4-nitrophenyl)prop-2-enenitrile. Comptes Rendus Chimie 18 (12), 1289–1296.

Iwan, A., Sek, D., 2011. Polymers with triphenylamine units: photonic and electroactive materials. Prog. Polym. Sci. 36 (10), 1277–1325.

Jeon, N.J., Lee, H.G., Kim, Y.C., Seo, J., Noh, J.H., Lee, J., Seok, S.I., 2014. o-Methoxy substituents in spiro-OMeTAD for efficient inorganic-organic hybrid perovskite solar cells. J. Am. Chem. Soc. 136 (22), 7837–7840.

Jeon, N.J., Lee, J., Noh, J.H., Nazeeruddin, M.K., Grätzel, M., Seok, S.I., 2013a. Efficient inorganic-organic hybrid perovskite solar cells based on pyrene arylamine derivatives as hole-transporting materials. J. Am. Chem. Soc. 135 (51), 19087–19090.

Jeon, N.J., Lee, J., Noh, J.H., Nazeeruddin, M.K., Grätzel, M., Seok, S.I., 2013b. Efficient inorganic–organic hybrid perovskite solar cells based on pyrene arylamine derivatives as hole-transporting materials. J. Am. Chem. Soc. 135 (51), 19087–19090.

Kang, M.S., Sung, S.D., Choi, I.T., Kim, H., Hong, M., Kim, J., Lee, W.I., Kim, H.K., 2015. Novel carbazole-based hole-transporting materials with star-shaped chemical structures for perovskite-sensitized solar cells. ACS Appl. Mater. Interfaces 7 (40), 22213–22217.

Kazim, S., Nazeeruddin, M.K., Grätzel, M., Ahmad, S., 2014. Perovskite as light harvester: a game changer in photovoltaics. Angew. Chem. Int. Ed. 53 (11), 2812–2824.

Kim, S.H., Choi, J., Sakong, C., Namgoong, J.W., Lee, W., Kim, D.H., Kim, B., Ko, M.J., Kim, J.P., 2015. The effect of the number, position, and shape of methoxy groups in triphenylamine donors on the performance of dye-sensitized solar cells. Dyes Pigm. 113, 390–401.

Krishnamoorthy, T., Kunwu, F., Boix, P.P., Li, H., Koh, T.M., Leong, W.L., Powar, S., Grimsdale, A., Grätzel, M., Mathews, N., 2014. A swivel-cruciform thiophene based hole-transporting material for efficient perovskite solar cells. J. Mater. Chem. A 2 (18), 6305–6309.

Kumar, P.S., Vasudevan, K., Prakasam, A., Geetha, M., Anbarasan, P.M., 2010. Quantum chemistry calculations of 3-phenoxyphthalonitrile dye sensitizer for solar cells. Spectrochim. Acta Part A: Mol. Biomol. Spectrosc. 77 (1), 45–50.

Laban, W.A., Etgar, L., 2013. Depleted hole conductor-free lead halide iodide heterojunction solar cells. Energy Environ. Sci. 6 (11), 3249–3253.

Lee, C., Yang, W., Parr, R.G., 1988. Development of the Colle-Salvetti correlation-energy formula into a functional of the electron density. Phys. Rev. B 37 (2), 785–789.

Lin, B.C., Cheng, C.P., Lao, Z.P.M., 2003. Reorganization energies in the transports of holes and electrons in organic amines in organic electroluminescence studied by density functional theory. J. Phys. Chem. A 107 (26), 5241–5251.

Liu, X., Kong, F., Ghadari, R., Jin, S., Yu, T., Chen, W., Liu, G., Tan, Z.A., Chen, J., Dai, S., 2017. Anthracene–arylamine hole transporting materials for perovskite solar cells. Chem. Commun. 53 (69), 9558–9561.

Liu, X., Zhu, L., Zhang, F., You, J., Xiao, Y., Li, D., Wang, S., Meng, Q., Li, X., 2016. Energy Technol.

Lou, Y.-H., Li, M., Wang, Z.-K., 2016. Seed-mediated superior organometal halide films by GeO2 nano-particles for high performance perovskite solar cells. Appl. Phys. Lett. 108, (5) 053301.

Lukeš, V., Aquino, A., Lischka, H., 2005. Theoretical study of vibrational and optical spectra of methylene-bridged oligofluorenes. J. Phys. Chem. A 109 (45), 10232–10238.

Frisch, M.J., Trucks, G.W., Schlegel, H.B., Scuseria, G.E., Robb, M. A., Cheeseman, J.R., Scalmani, G., Barone, V., Petersson, G.A., Nakatsuji, H., Li, X., Caricato, M., Marenich, A., Bloino, J., Janesko, B.G., Gomperts, R., Mennucci, B., Hratchian, H.P., Ortiz, J.V., Izmaylov, A.F., Sonnenberg, J.L., Williams-Young, D., Ding, F., Lipparini, F., Egidi, F., Goings, J., Peng, B., Petrone, A., Henderson, T., Ranasinghe, D., Zakrzewski, V.G., Gao, J., Rega, N., Zheng, G., Liang, W., Hada, M., Ehara, M., Toyota, K., Fukuda, R., Hasegawa, J., Ishida, M., Nakajima, T., Honda, Y., Kitao, O., Nakai, H., Vreven, T., Throssell, K., Montgomery Jr., J. A., Peralta, J.E., Ogliaro, F., Bearpark, M., Heyd, J.J., Brothers, E., Kudin, K.N., Staroverov, V.N., Keith, T., Kobayashi, R., Normand, J., Raghavachari, K., Rendell, A., Burant, J.C., Iyengar, S.S., Tomasi, J., Cossi, M., Millam, J.M., Klene, M., Adamo, C., Cammi, R., Ochterski, J.W., Martin, R.L., Morokuma, K., Farkas, O., Foresman, J.B., Fox, D.J., 2016. Gaussian 09. Gaussian, Inc., Wallingford CT.

Mandal, S., Rao, S., Ramanujam, K., 2017. Understanding the photo-electrochemistry of metal-free di and tri substituted thiophene-based organic dyes in dye-sensitized solar cells using DFT/TD-DFT studies. Ionics.

Meng, L., Zhao-Kui, W., Ying-Guo, Y., Yun, H., Shang-Lei, F., Jin-Miao, W., Xing-Yu, G., Liang-Sheng, L., 2016. Copper salts doped spiro-OMeTAD for high-performance perovskite solar cells. Adv. Energy Mater. 6 (21), 1601156.

Minaev, B.F., Baryshnikov, G.V., Minaeva, V.A., 2012. Electronic structure and spectral properties of the triarylamine-dithienosilole dyes for efficient organic solar cells. Dyes Pigm. 92 (1), 531–536.

Nelsen, S.F., Trieber, D.A., Ismagilov, R.F., Teki, Y., 2001. Solvent effects on charge transfer bands of nitrogen-centered intervalence compounds. J. Am. Chem. Soc. 123 (24), 5684–5694.

Norton, J.E., Brédas, J.-L., 2008. Polarization energies in oligoacene semiconductor crystals. J. Am. Chem. Soc. 130 (37), 12377–12384.

Pogantsch, A., Heimel, G., Zojer, E., 2002. Quantitative prediction of optical excitations in conjugated organic oligomers: a density functional theory study. J. Chem. Phys. 117 (12), 5921–5928.

Rakstys, K., Abate, A., Dar, M.I., Gao, P., Jankauskas, V., Jacopin, G., Kamarauskas, E., Kazim, S., Ahmad, S., Grätzel, M., Nazeeruddin, M.K., 2015. Triazatruxene-based hole transporting materials for highly efficient perovskite solar cells. J. Am. Chem. Soc. 137 (51), 16172–16178.

Roy, Dennington, Keith, T., Millam, J., 2009. GaussView. S. Mission. KS, Semichem Inc.

Salunke, J.K., Wong, F., Feron, K., Manzhos, S., Lo, M.F., Shinde, D., Patil, A., Lee, C., Roy, V., Sonar, P., 2016. Phenothiazine and carbazole substituted pyrene based electroluminescent organic semiconductors for OLED devices. J. Mater. Chem. C 4 (5), 1009–1018.

Shi, D., Qin, X., Li, Y., He, Y., Zhong, C., Pan, J., Dong, H., Xu, W., Li, T., Hu, W., Brédas, J.-L., Bakr, O.M., 2016. Spiro-OMeTAD single crystals: remarkably enhanced charge-carrier transport via mesoscale ordering. Sci. Adv. 2 (4).

Stranks, S.D., Eperon, G.E., Grancini, G., Menelaou, C., Alcocer, M. J., Leijtens, T., Herz, L.M., Petrozza, A., Snaith, H.J., 2013. Electron-hole diffusion lengths exceeding 1 micrometer in an organometal trihalide perovskite absorber. Science 342 (6156), 341–344.

Vivo, P., Salunke, J.K., Priimagi, A., 2017. Hole-transporting materials for printable perovskite solar cells. Materials 10 (9), 1087.

Wang, H., Sheikh, A.D., Feng, Q., Li, F., Chen, Y., Yu, W., Alarousu, E., Ma, C., Haque, M.A., Shi, D., Wang, Z.-S., Mohammed, O.F., Bakr, O.M., Wu, T., 2015. Facile synthesis and high performance of a new carbazole-based hole-transporting material for hybrid perovskite solar cells. ACS Photonics 2 (7), 849–855.

Wang, J., Chen, Y., Li, F., Zong, X., Guo, J., Sun, Z., Xue, S., 2016a. A new carbazole-based hole-transporting material with low dopant content for perovskite solar cells. Electrochim. Acta 210, 673–680.

Wang, Z.-K., Gong, X., Li, M., Hu, Y., Wang, J.-M., Ma, H., Liao, L.-S., 2016b. Induced crystallization of perovskites by a perylene underlayer for high-performance solar cells. ACS Nano 10 (5), 5479–5489.

Wazzan, N., El-Shishtawy, R.M., Irfan, A., 2017. DFT and TD–DFT calculations of the electronic structures and photophysical properties of newly designed pyrene-core arylamine derivatives as hole-transporting materials for perovskite solar cells. Theor. Chem. Acc. 137 (1), 9.

Wazzan, N., El-Shishtawy, R.M., Irfan, A., 2018. DFT and TD–DFT calculations of the electronic structures and photophysical properties of newly designed pyrene-core arylamine derivatives as hole-transporting materials for perovskite solar cells. Theor. Chem. Acc. 137 (1), 9.

Yang, W.S., Noh, J.H., Jeon, N.J., Kim, Y.C., Ryu, S., Seo, J., Seok, S.I., 2015. High-performance photovoltaic perovskite layers fabricated through intramolecular exchange. Science 348 (6240), 1234–1237.

Yu, Z., Sun, L., 2015. Recent progress on hole-transporting materials for emerging organometal halide perovskite solar cells. Adv. Energy Mater. 5 (12).

Zhang, Y., Li, Y., Chen, C., Wang, L., Zhang, J., 2017a. Design new hole transport materials for efficient perovskite solar cells by suitable combination of donor and core groups. Org. Electron. 49, 255–261.

Zhang, Y., Li, Y., Chen, C., Wang, L., Zhang, J., 2017b. Design new hole transport materials for efficient perovskite solar cells by suitable combination of donor and core groups. Org. Electron. 49 (Supplement C), 255–261.

Zhang, Y., Zhang, L., Wang, R., Pan, X., 2012a. Theoretical study on the electronic structure and optical properties of carbazole-π-dimesitylborane as bipolar fluorophores for nondoped blue OLEDs. J. Mol. Graph. Model. 34, 46–56.

Zhang, Z.-L., Zou, L.-Y., Ren, A.-M., Min, C.-G., Sun, Y., Liu, Y.-F., 2012b. Theoretical investigations on electronic structures and photophysical properties of novel bridged triphenylamine derivatives. Int. J. Quantum Chem. 112 (5), 1473–1490.

Zhao, C., Wang, W., Ma, Y., 2013. Molecular design toward good hole transport materials based on anthra[2,3-c]thiophene: a theoretical investigation. Comput. Theor. Chem. 1010, 25–31.

Zhu, L., Shan, Y., Wang, R., Liu, D., Zhong, C., Song, Q., Wu, F., 2017. High-efficiency perovskite solar cells based on new type compounds as hole transport materials: the role of 2, 7-and 3, 6-substituted carbazole derivatives. Chem. – A Eur. J. 23 (18), 4373–4379.

Zhurko, G., Zhurko, D., 2009. Chemcraft program, Academic version 1.8.